Journal of Nanobiotechnology

RESEARCH

Open Access

pH-responsive cationic polymer-functionalized poly-ε-caprolactone microspheres scavenge cell-free-DNA to alleviate intestinal ischemia/reperfusion injury by inhibiting M1 macrophage polarization

Hanbin Xie[1†], Cong Wei[2†], Chang Xiong[1†], Ziyan Huang[3†], Chaojin Chen[1], Xue Xiao[1], Linan Zhang[1], Zhenjia Lin[1], Weifeng Yao[1*], Tianyu Zhao[2*] and Ziqing Hei[1,4*]

Abstract

Intestinal ischemia/reperfusion (I/R) injury is a common life-threatening condition. Inflammatory dysregulation plays a crucial role in the pathological progression of intestinal I/R injury, indicating that controlling excessive inflammatory responses can be an effective strategy for mitigating I/R injury. Herein, after establishing a correlation between cell-free DNA (cfDNA) levels and postoperative inflammatory factors in samples from patients with intestinal I/R, we tested a cfDNA-scavenging approach for the treatment of intestinal I/R injury. Poly-ε-caprolactone (PCL) microspheres (Micro DEA2k) functionalized with a pH-responsive cationic polymer (DEA2k) to efficiently scavenge cfDNA were synthesized and evaluated.These microspheres exhibited enhanced cfDNA adsorption under inflammation-induced acidic conditions, along with low toxicity, reduced non-specific protein binding, and extended peritoneal retention. In a mouse model of intestinal I/R injury, the intraperitoneal injection Micro DEA2k effectively bound cfDNA, regulated the mononuclear phagocytic system, decreased the number of M1 macrophages, suppressed inflammation, and significantly improved the survival rate of the mice. These findings suggest that cfDNA scavenging using cationic microspheres has considerable potential for alleviating intestinal I/R injury.

†Hanbin Xie, Cong Wei, Chang Xiong and Ziyan Huang contributed equally to this work.

*Correspondence:
Weifeng Yao
yaowf3@mail.sysu.edu.cn
Tianyu Zhao
zhaoty25@mail.sysu.edu.cn
Ziqing Hei
heizq@mail.sysu.edu.cn

Full list of author information is available at the end of the article

Graphical Abstract

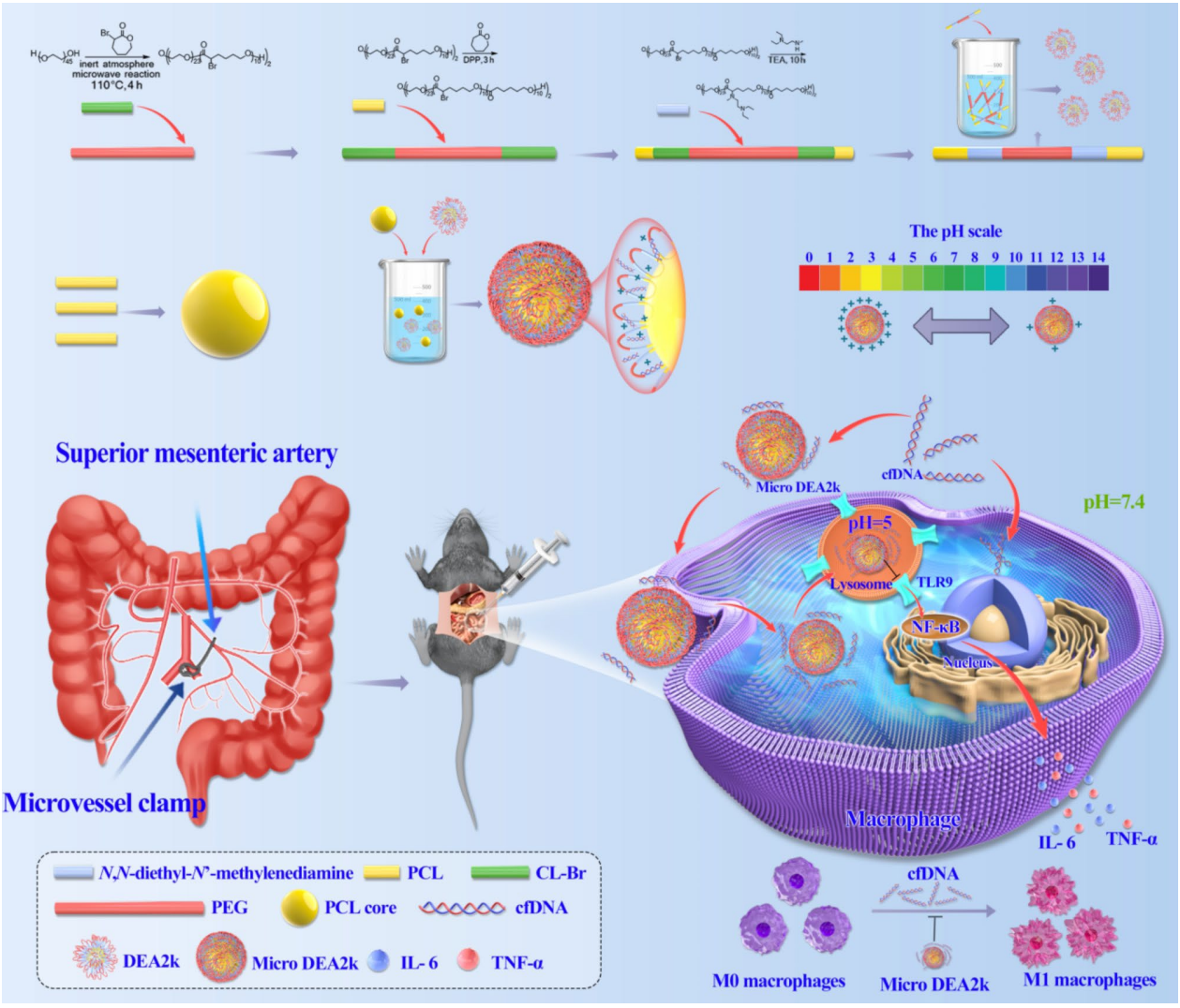

Keywords Cell-free DNA scavenging, Cationic microparticles, Ischemia/reperfusion injury, Macrophage

Introduction

Intestinal ischemia/reperfusion (I/R) injury constitutes a common and challenging clinical condition that may manifest during shock, severe trauma, intestinal injury, or laparoscopic surgery [1–3]. During the ischemic phase, enterocytes undergo necrosis due to mitochondrial dysfunction and metabolic derangements. Upon reperfusion, these compromised intestinal cells release damage-associated molecular patterns (DAMPs), which elicit a substantial infiltration of immune cells and subsequently lead to inflammatory dysregulation [4, 5]. This, in turn, further undermines the structural and functional integrity of the mechanical, chemical, immune, and biological barriers of the intestinal mucosa, thereby making the patient more susceptible to systemic inflammatory response syndrome (SIRS) and multiple organ dysfunction syndrome (MODS) [6].

Cell-free DNA (cfDNA), a DAMP released by dead cells, can be internalized by immune cells (e.g., macrophages) and trigger inflammatory dysregulation through the activation of toll-like receptors (TLRs) [7]. In recent years, increasing evidence has suggested that cfDNA levels increase significantly in various organs following I/R injury. Schütz et al. found that the level of cfDNA in the body can increase by more than 50% on the first day after liver transplantation, whereas in acute cardiovascular events, large amounts of cfDNA can be produced and released into the blood during I/R [8, 9]. Our study has also shown that

cfDNA levels are significantly upregulated both in patients undergoing laparoscopic surgery and in mouse models of intestinal I/R injury, and are strongly correlated with inflammatory factors and the severity of intestinal injury. Hence, increased cfDNA serves not only as a potential marker for identifying organ injury but also as a proinflammatory mediator that exacerbates damage. This makes the clearance or neutralization of cfDNA a promising strategy for the treatment of intestinal injuries following I/R.

Deoxyribonuclease I (DNase-1) for cfDNA clearance has demonstrated good therapeutic efficacy in diseases such as sepsis and I/R injury [10, 11]. However, the systemic administration and potential side effects of DNase-1 have restricted its clinical application. Therefore, in recent years, researchers have focused on bionanomaterials, especially cationic nanoparticles, that can adsorb negatively charged cfDNA, thereby enabling their clearance. To date, different types of cationic bionanomaterials have been designed for the treatment of diseases such as rheumatoid arthritis, sepsis, acute kidney injury, and periodontitis [7, 12–14]. Encouragingly, these bio-nanomaterials have demonstrated considerable cfDNA scavenging ability and good biocompatibility. However, traditional cationic nanoparticles can bind non-specifically to negatively charged proteins, resulting in incomplete cfDNA clearance and unstable treatment effects, whereas cfDNA scavengers can have different administration routes and mechanisms of action across different types of diseases [15]. Therefore, cfDNA- scavenging nanomaterials that specifically target the intestinal I/R injury need to be developed.

In this study, to obtain a safe, effective, and long-lasting cfDNA clearance material, we initially selected poly-ε-caprolactone (PCL) and polyethylene glycol (PEG), which are Food and Drug Administration (FDA)-approved materials, as the backbone. The PEG and PCL block copolymers can self-assemble into PCL-b-PEG-b-PCL nanoparticles (PCEC), which have excellent biocompatibility and a wide range of applications. Considering the acidic microenvironment characteristic of inflammation [16], we ionized PCEC by carrying tertiary amine functional groups with thiols or secondary amines, thereby preparing the pH-responsive polymer material, which we have termed DEA2k. Here, DEA denotes diethylamine-modified PCL/PEG block polymer, and 2k refers to polyethylene glycol with a molecular weight of 2000; further, by assembling DEA2k onto the surface of PCL particles, we prepared larger volume cationic microparticles (cMPs) to increase the residence time at the inflammatory site. Therefore, we developed a novel micrometer-scale pH-responsive cMP, termed Micro DEA2k. These microparticles exhibit a strong cfDNA-binding ability in acidic environments with greatly reduced cytotoxicity. Moreover, Micro DEA2k has an enhanced retention effect and can remain in the inflammatory region for a prolonged period locally to remove cfDNA. Most importantly, Micro DEA2k can avoid permeation into other organs, thereby possessing high biocompatibility and making it a promising candidate for clinical application.

In summary, we found that cfDNA was involved in intestinal I/R injury, which led us to develop a pH-responsive cMP with good accumulation and retention abilities. These cMPs can remove cfDNA and inhibit the polarization of M1 macrophages by the TLR9-NF-κB signaling pathway, thereby reducing both local and systemic inflammatory responses, improving the survival rate of mice with intestinal I/R injury, and alleviating multi-organ damage (Scheme 1). This study presents a feasible method for cfDNA clearance, that is safe, effective, and promising for clinical applications.

Materials and methods

Patient sample collection and data recording

Ten patients who underwent laparoscopic gastrointestinal surgery were included in this study. The patient recruitment was approved by the Ethics Committee of the Third Affiliated Hospital of Sun Yat-sen University (II2023-272-01). Samples of peritoneal drainage fluid and blood were collected from patients immediately and 6 h after surgery for analysis. To minimize the risk of blood contamination, we specifically selected drainage fluid that was distant from the abdominal incision drainage tube. Furthermore, to ensure that the sample remained unaffected by blood cells, we promptly subjected the collected drainage fluid to low-temperature centrifugation and subsequently stored it at -80℃. The operative duration was recorded from the surgical anesthesia center system, and the time of the first postoperative flatus was obtained from the gastrointestinal surgery nursing system.

Establishment and treatment of the mouse intestinal I/R injury model

This animal study was approved by the Animal Ethics Committee of the South China Agricultural University (2023F202). Male C57BL/6J mice (6–8 weeks old) were purchased from the Animal Center of South China Agricultural University. The animals were housed under specific pathogen-free conditions with a standard 12/12 h light/dark cycle. The mice fasted the night before the experiment but were permitted free access to water. The experimental groups were as follows: sham, I/R, and Micro DEA2k. With reference to the literature, after the mice were anesthetized with 1% isoflurane (Shenzhen RWD Life Science), a midline incision was made, the layers were opened, and the superior mesenteric artery (SMA) was isolated. A noninvasive microvascular arterial clamp was used to occlude the SMA for 45 min, after which the clamp was removed to restore SMA blood flow

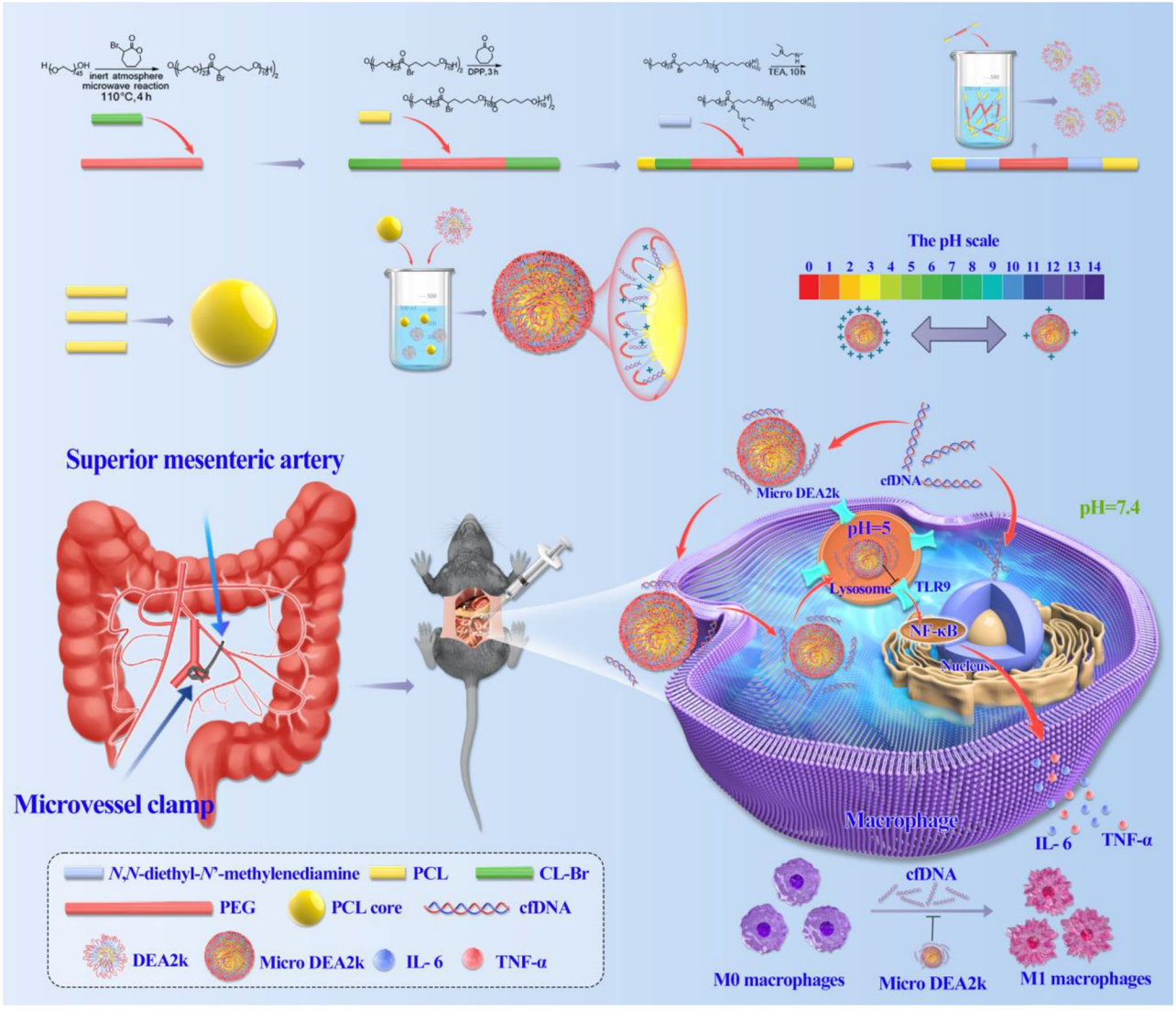

Fig. 1 Schematic diagram of the synthesis of Micro DEA2k and its adsorption of cfDNA to alleviate intestinal I/R injury. After intraperitoneal injection of pH-responsive Micro DEA2k, it adsorbs cfDNA and inhibits M1 polarization of macrophages through the TLR9-NF-κB signaling pathway, resulting in reduced release of inflammatory cytokines and thereby alleviating intestinal injury and systemic inflammatory responses

[17, 18]. The abdominal incision was closed with continuous sutures using 3 – 0 silk thread. For the Micro DEA2k (0.4 mg/mL) group, 1 mL was injected intraperitoneally before closing the incision. The I/R group was intraperitoneally injected with an equal volume of 1× phosphate buffered saline (PBS) (ProCell). For the Sham group, the SMA was isolated without clamping. Immediately after surgery, each mouse was injected subcutaneously with preheated sterile saline (0.5 mL) for fluid resuscitation and was kept warm using a heating pad. Mice were monitored for 24 h to record their survival rates. Clinical scoring was also performed based on the following criteria: 0, no symptoms; 1, piloerection and huddling; 2, piloerection, huddling, and diarrhea; 3, lack of interest in the surroundings and severe diarrhea; 4, reduced movement and lethargy; and 5, loss of self-righting reflexes [19]. The mice were humanely euthanized at a score of 5.

Molecular docking

The Drew-Dickerson dodecamer (1BNA) was used as the DNA model for molecular docking. Its crystal structure file was obtained from the Protein Data Bank database, which was saved as a pdbqt file after removing water molecules and adding hydrogen using AutoDock 4.2.6 and AutoDockTools 1.5.7 [20, 21]. Two consecutive repeating units of the cation segment were selected as the model ligands. After MM2 energy minimization, they were converted into pdb format using OpenBabel 3.1.1 (with an extra setting of hydrogen addition at pH = 1 for the protonated ligand model) and imported into AutoDockTools

1.5.7, where Gasteiger charges were added after the addition of hydrogen. After setting the torsional bonds and torsional centers, the file was exported as a pdbqt file. The size of the lattice point region was set to 60 nm × 80 nm × 120 nm, such that the docking active site spanned the entire DNA molecular model, with a spacing of 0.375 Å. After exporting the gpf file, AutoGrid was used to perform lattice point calculations. The parameters related to molecular docking were set using a genetic algorithm (GA) to generate 100 final conformations. Each run had a maximum energy evaluation of 2.5 million times and a maximum number of steps of 27,000, with all other parameters retaining their default system settings. In the docking run options, parameters such as random number generation, energy, step size, and export format were retained at their default settings. The dpf file was exported using the Lamarckian GA. Finally, the dpf file was used to perform molecular docking, and the molecular docking binding energies were calculated using the dlg file. The binding pose with the lowest energy was selected and visualized using UCSF Chimera 1.16. The unbound state is defined as the state in which the ligand reaches equal free energy at different positions when it is far away from the receptor, and it can be assumed that no interaction occurs between the receptor and ligand.

Synthesis of DEA2k and Micro DEA2k

Synthesis of α-bromo-Ɛ-caprolactone (CL-Br). Initially, 57.12 g of *N*-bromosuccinimide (NBS, 99.00%, Aladdin) and 5.81 g of *p*-toluenesulfonic acid (98.5%, Aladdin) were dissolved in 200 mL of dichloromethane (DCM, 99.5%, Guanghua Sci-Tech) and stirred in an ice-water bath. Then, 30.00 g of cyclohexanone (99.0%, Macklin) was added dropwise. The mixture was subjected to cold vacuum filtration to remove the salts, followed by extraction and washing. The extraction was performed using a saturated sodium chloride solution, followed by washing and drying over anhydrous sodium sulfate to obtain 38.52 g of 2-bromocyclohexanone. Next, the 2-bromocyclohexanone was dissolved in 250 mL of DCM, and m-chloroperoxybenzoic acid (mCPBA, 55.07 g, 239.35 mmol) was added. The mixture was refluxed overnight at 50 °C and then cooled. The solution was extracted with saturated sodium thiosulfate solution, saturated sodium bicarbonate solution, and deionized water. It was then extracted with saturated sodium chloride solution to remove water and dried over anhydrous sodium sulfate overnight. The resulting crystals were recrystallized from a DCM/n-hexane mixture at -20 °C to obtain 23.48 g of white crystals, identified as CL-Br. The product was placed in a microwave reactor (Initiator+, Biotage) with 3.41 g of the macroinitiator PEG (average Mn 2000, Aladdin) and reacted at 110 °C for 4 h for ring-opening polymerization (ROP), which produced 8.84 g of the triblock copolymer P(CL-Br)-b-PEG-b-P(CL-Br). Following this process, the triblock copolymer initiated ROP in 2.57 g of ε-caprolactone (97%, Bide Pharmatech), which yielded the pentablock copolymer PCL-b-P(CL-Br)-b-PEG-b-P(CL-Br)-b-PCL. Next, 2 g of the pentablock copolymer was weighed and modified by adding 1.51 g of N, N-diethyl-N'-methyl ethylenediamine (98%, Macklin); the resulting product was named DEA2k. After 1 mg/mL of DEA2k was mixed evenly with 1 mg/mL of PCL microspheres, centrifugation was performed using a tabletop centrifuge (Centrifuge 5810R, Eppendorf) at 15,000 rpm for 10 s to precipitate the microspheres. The supernatant containing free DEA2k was removed. The mass m_m of the microspheres was obtained by lyophilization using the weight reduction method, and the total mass m_t was obtained by lyophilization after direct mixing. The surface polymer content per unit mass of microspheres was calculated to be 85.7% using the following formula:

$$\frac{2m_{m-m_t}}{m_t} \times \ 100\% \tag{1}$$

The vast majority of the polymers were successfully attached to the surface of the microspheres, and the product was named Micro DEA2k.

Characterization of DEA2k and Micro DEA2k

Proton nuclear magnetic resonance (NMR) spectra were recorded at room temperature using an NMR spectrometer (AVANCE III 400 MHz, Bruker). The relative molecular weight and dispersity were measured by gel permeation chromatography (GPC) (1260 Infinity, Agilent). The morphology was characterized using transmission electron microscopy (TEM, JEOL1400+). The hydrated size (Size), polydispersity index (PDI), and zeta potential were measured by dynamic light scattering (DLS, Malvern Zetasizer Nano ZS) at 25 °C.

In vitro cytotoxicity assay

RAW264.7 cells, purchased from the ATCC cell bank, were cultured in Dulbecco's modified Eagle's medium (DMEM; Gibco Life Technologies), which contained 10% fetal bovine serum (FBS; Gibco Life Technologies) and 1% bispecific antibody (Pen Strep, Penicillin Streptomycin, Gibco) in an incubator (Steri-Cycle 371, Thermo Scientific) at 37 °C and 5% carbon dioxide. Cells in good condition were selected and seeded into a 96-well plate at approximately 10^4 cells per well. After culturing overnight, the culture medium was replaced with fresh medium containing different concentrations of cationic polymers. After 24 h of incubation, 10 μL of 5 mg/mL methylthiazolyldiphenyl-tetrazolium bromide solution (MTT, 98%, Sigma-Aldrich) was added and incubated for another 4 h. After removing the supernatant,

10 μL of dimethyl sulfoxide (DMSO, 99.7%, Guangzhou Chemical Reagent Factory) was added to each well to dissolve the pellet. Finally, the absorbance was measured at 570 nm using a microplate reader (BioTek Synergy2 Gen 5). The cell survival rate was calculated by $(Q–Q_0)/(Q_1–Q_0)\times100\%$, where Q is the optical density (OD) of cells with the polymer, Q_0 is the OD of wells without cells, and Q_1 is the OD of cells without the polymer. Each experiment was repeated three times. The IC50 was calculated by fitting a logistic equation.

Protein adsorption capacity assay

Resistance to protein adsorption was assessed using the BCA Protein Assay Kit (Pierce™ BCA Protein Assay Kit, Thermo Scientific). Firstly, 50 μL of 2 mg/mL bovine serum albumin (BSA, Aladdin) solution was mixed evenly with 50 μL of 1 mg/mL cationic material. The control group was established by mixing 50 μL of deionized water with 50 μL of BSA solution. After incubation at 37 °C in a shaker for 1 h, the samples were centrifuged at 8000 rpm for 5 min, and the supernatant was collected. Calibration curves were obtained for BSA solutions with different concentrations, and the residual BSA concentration in the sample supernatant was determined based on ultraviolet absorption (280 nm). The amount of BSA adsorbed onto the cationic polymer was calculated using $(C_C–C_T)V/m$, where C_C is the BSA concentration of the control group (1 mg/mL), C_T is the BSA concentration of the supernatant after the addition of the cationic polymer, V is the volume of the solution (100 μL), and m is the weight of the cationic polymer (50 μg). Each experiment was repeated three times.

Potentiometric acid-base titration

DEA2k was dissolved in 10 mL of hydrochloric acid standard solution to yield a concentration of 500 μM (amine group content: 10 mM), and 0.1 M sodium hydroxide standard solution was gradually added dropwise to yield a pH of 2.00; this served as the starting point for the titration. Next, a 0.1 M sodium hydroxide standard solution was added dropwise with constant stirring, and the cumulative amount of sodium hydroxide solution added and the corresponding pH value were measured, and the titration curve was plotted. The peak of the first-order derivative of the curve is the point of sudden pH change, defined as the starting and ending points of amine protonation. The relationship between the degree of protonation α and pH during the process was calculated by using the following equation:

$$\alpha = \frac{\left(V_t - \frac{(\Phi_t+\Phi)\Delta V_t}{\Delta pH_t}\right) - V}{\left(V_t - \frac{(\Phi_t+\Phi)\Delta V_t}{\Delta \Phi_t}\right) - \left(V_i - \frac{(\Phi_i+\Phi)\Delta V_i}{\Delta \Phi_t}\right)} \quad (2)$$

where Φ is the pH value of the solution, V is the cumulative volume of sodium hydroxide solution added at that pH, and subscripts i and t denote the starting and ending points of deprotonation, respectively. The protonation curve of the cationic polymer was fitted by a combination of two logistic equations, calculated as follows:

$$\alpha = E\left(1 - \frac{1}{1+\left(\frac{\Phi}{C_1}\right)^{B_1}}\right) + (1-E)\left(1 - \frac{1}{1+\left(\frac{\Phi}{C_2}\right)^{B_2}}\right), \quad (3)$$

where B_1 and C_1 correspond to easier-to-protonate amine groups, B_2 and C_2 correspond to harder-to-protonate amine groups, and E represents the proportion of easier-to-protonate amine groups. The buffer capacity (β) at different pH values can be calculated from the fitted degree of protonation of the cationic polymer, and the formula is as follows:

$$\beta = (V_t - V_i - \frac{(\Phi_t - \Phi)\Delta V_t}{\Delta \Phi_t} - \frac{(\Phi - \Phi_i)\Delta V_i}{\Delta \Phi_i})\frac{\Delta \alpha}{\Delta \Phi} \quad (4)$$

Measurement of DNA binding capacity

The binding capacity of the cationic polymer to CpG1826 was measured by agarose gel electrophoresis. Cationic polymer solutions with different concentrations were mixed with 0.4 μL of 1 mg/mL CpG1826 solution (ODN 1826, 5'-tccatgacgttcctgacgtt-3', GenScript) to obtain complex solutions with different nitrogen-to-phosphorus ratios, and the CpG1826 aqueous solution was used as a blank control. After allowing the solutions to stand at room temperature for 0.5 h, they were added to 2 μL of 1% agarose gel containing a nucleic acid dye (Goldview nucleic acid dye (10,000 × DMSO), Biosharp, China). Electrophoresis was performed in 1% tris-acetate-EDTA (TAE) buffer solution (voltage 60 V, 45 min, DYY-6 C, Beijing Liuyi). Finally, the gels were photographed and analyzed using a gel imaging system (Gel Doc XR+; Bio-Rad).

The binding capacity of the cationic polymer was quantitatively assessed by competitive binding to ethidium bromide (EtBr). Firstly, 2.17 μL of 1 mg/mL EtBr (94%, Acros Organics) was added to 3 mL of PBS or sodium acetate buffered solution (SABS) to simulate different pH values, and the fluorescence emission spectrum of the solution was measured. Then, 10 μL of 1 mg/mL ctDNA (Sigma-Aldrich) solution was added and mixed evenly to increase the fluorescence intensity of the solution. Subsequently, different volumes of cationic polymer solution (1 mg/mL) were added sequentially and mixed. The fluorescence emission curve was measured using a fluorescence spectrometer (excitation wavelength: 280 nm, detection emission wavelength: 500–800 nm).

In vitro anti-inflammatory assay

RAW264.7 macrophages were added to 96-well plates at a density of 1×10^4 cells/well. Cells were cultured in DMEM containing 10% FBS for 12 h. The culture medium was replaced with fresh medium containing CpG1826 (0.5 μM), and the cells were co-cultured for 4 h before discarding the medium. After washing three times with PBS, fresh medium containing cationic polymer (25 μg/mL) was added, and the cells were incubated for 24 h. Then, the supernatant was collected for TNF-α and IL-6 assays. The group without CpG1826 and cationic polymer in the medium served as the control group.

Western blot

RAW264.7 macrophages were added to 6-well plates at a density of 2×10^5 cells/well. Cells were cultured in DMEM containing 10% FBS for 12 h. The culture medium was replaced with fresh medium containing CpG1826 (0.5 μM), and the cells were co-cultured for 4 h before discarding the medium. After washing three times with PBS, fresh medium containing cationic polymer (25 μg/mL) was added, and the cells were incubated for 24 h. Centrifugation was performed to collect the cells, and RIPA lysis buffer (Beijing Solarbio Technology Co., Ltd.) was added, boiled, and centrifuged. The supernatant was collected to obtain the protein samples. The different protein samples were separated by 10% sodium dodecyl sulfate polyacrylamide gel electrophoresis (SDS-PAGE), and the proteins on the PAGE gel were transferred to polyvinylidene fluoride (PVDF) membranes. The PVDF membrane bands of the corresponding protein molecular weights and appropriate sizes were excised and blocked in a solution of skim milk powder for 1 h. Then, they were incubated overnight on a shaker at 4 °C with the following primary antibodies: anti-p65 (1:1000) (Cell Signaling Technology, 8242 S, USA), anti-pp65 (1:1000) (Cell Signaling Technology, 3033 S, USA), anti-TLR9 (1:1000) (ABclonal, A14642, China), anti-MyD88 (1:1000) (ABclonal, A0980, China), and anti-β-actin (1:50000) (ABclonal, AC026, China). After the primary antibodies were recovered, the samples were washed thrice with tris-buffered saline with Tween 20 (TBST) solution (Biosharp, BL315B, China) for 6 min each and incubated with an anti-rabbit IgG secondary antibody (1:20000) (Cell Signaling Technology, 7074 S, USA) at room temperature for 1 h. After discarding the secondary antibody, the samples were washed three times with TBST for 6 min each, and enhanced chemiluminescence (ECL) exposure solution (Shanghai Beyotime Biotechnology Co., Ltd.) was added dropwise for imaging.

Confocal laser scanning microscopy

RAW264.7 macrophages were seeded at a concentration of 4×10^5/mL in glass-bottom confocal dishes and incubated overnight. After washing three times with PBS, serum-free DMEM was added, which contained 0.5 μM FAM fluorescently labeled CpG1826 (FAM-CpG1826, GenScript Biotech). After co-culturing for 4 h, the cells were washed three times with PBS, and serum-free DMEM was added, which contained 25 μg/mL Micro DEA2k. After culturing for another 4 h, the medium was discarded and the cells were washed three times with PBS. Next, the cells were incubated with 0.2/mL of lysosomal green fluorescent probe (LysoTracker™ Green DND-99, Invitrogen) in serum-free DMEM for 30 min in the dark, followed by 1 μg/mL of bisbenzimide H 33,342 trihydrochloride (Hoechst 33342, Sigma) in PBS for 10 min in the dark for staining. The colocalization of lysosomes, CpG1826, and Micro DEA2k was analyzed using a laser confocal microscope (TCS SP8, Leica Microsystems, GmbH).

cfDNA purification and quantification

cfDNA was purified from serum, peritoneal drainage, and lavage fluid using a DNA purification kit (PCR Purification Kit/DNA Purification Kit, D0033, Shanghai Beyotime Biotechnology Co., Ltd.), and the concentration of cfDNA was measured using an ultra-micro spectrophotometer (Thermo NanoDrop 2000, Thermo Fisher Scientific Inc.).

HE staining

After fixation for 24 h, the tissue samples were embedded in paraffin and sectioned using a paraffin microtome (Leica) to obtain tissue sections with a thickness of 2 μm. Sections were deparaffinized, stained with hematoxylin and eosin (HE), washed, dehydrated, and mounted. Routine HE staining was used to assess the histomorphological changes in major organs, and an intelligent pathology imaging system microscope (Vectra, PerkinElmer) was used for image acquisition and analysis. The degree of small intestinal injury after reperfusion was assessed using the modified Chiu's method, which is based on changes in the intestinal mucosal villi and glands [22]. The histological damage to the lungs, kidneys, and liver was assessed using their respective scoring systems [23–25]. Automated image analysis was performed on five randomly selected 200× magnification images from each sample.

Immunohistochemistry

After preparing paraffin sections according to the steps above, the expression and location of F4/80 were detected using a primary anti-F4/80 antibody (1:500) (GB113373, Servicebio) and a labeled goat anti-rabbit secondary antibody (1:200) (GB23303, Servicebio). The expression and localization of TLR9 were detected using a primary anti-TLR9 antibody (1:300) and a labeled goat anti-rabbit

secondary antibody (1:200) (GB23303, Servicebio). The expression and location of MyD88 were detected using a primary anti-MyD88 antibody (1:1000) (GB111554, Servicebio) and a labeled goat anti-rabbit secondary antibody (1:200) (GB23303, Servicebio). The expression and localization of p65 were detected using a primary anti-p65 antibody (1:500) (#8242, Abcam) and labeled goat anti-rabbit secondary antibody (1:200) (GB23303, Servicebio). Finally, using an intelligent pathology imaging system microscope (Vectra, PerkinElmer) for image acquisition and analysis, automated image analysis was performed on five randomly selected 200× images from each sample to quantify the relative intensities of protein staining for F4/80, TLR9, MyD88, and p65.

Enzyme-linked immunosorbent assay

The concentrations of TNF-α and IL-6 in the culture supernatant of RAW 264.7 cells were measured using the Mouse TNF-α Enzyme-Linked Immunosorbent Assay (ELISA) Kit (JL10484) and the Mouse IL-6 ELISA Kit (JL20268), respectively. The concentrations of TNF-α, IL-6 and MCP-1 in mouse serum and peritoneal lavage fluid were measured using the Mouse TNF-α ELISA Kit (JL10484), Mouse IL-6 ELISA Kit (JL20268), and Mouse MCP-1 ELISA Kit (JL20304), respectively. The concentrations of LPS and FABP2 in the mouse serum were determined using mouse LPS ELISA kits (JL20691) and mouse FABP2 ELISA kits (JL20694). All the reagents were sourced from Shanghai Jianglai Biotechnology Co., Ltd.

Analysis of biochemical parameters

Serum creatinine (CRE) content was calculated by measuring the absorbance at 546 nm using a Mouse Creatinine Assay Kit (Sarcosine Oxidase Method; JL-T0928, Shanghai Jianglai Biotechnology Co., Ltd.). Serum blood urea nitrogen (BUN) content was calculated by measuring the absorbance at OD = 625 nm using a Mouse Urea Nitrogen Assay Kit (Enzyme Method; JL-T1014, Shanghai Jianglai Biotechnology Co, Ltd). Serum alanine aminotransferase and aspartate aminotransferase (ALT/AST) levels were calculated by measuring the absorbance at 340 nm using a Mouse Serum ALT/AST Assay Kit (JL-T2637, Shanghai Jianglai Biotechnology Co, Ltd.).

Flow cytometry analysis

RAW264.7 macrophages were added to 6-well plates at a density of 2×10^5 cells/well. Cells were cultured in DMEM containing 10% FBS for 12 h. The culture medium was replaced with fresh medium containing CpG1826 (0.5 μM), and the cells were co-cultured for 4 h before discarding the medium. After washing three times with PBS, fresh medium containing cationic polymer (25 μg/mL) was added, and the cells were incubated for 24 h, then centrifuged and resuspended. The cells were then treated with a viability dye (1:500) (423101, Biolegend), blocked with CD16/32 (1:50) (101302, Biolegend), and stained with a CD86 antibody (1:80) (105012, Biolegend).

Peritoneal lavage fluid was collected 6 h after reperfusion using the method described above and centrifuged to obtain a single-cell suspension. The supernatant was discarded, leaving the cell pellet, which was treated with a viability dye (1:500) (423101, BioLegend) and blocked with CD16/32 (1:50) (101302, BioLegend). This was followed by staining with mouse CD45 (1:80) (103154, BioLegend, USA), F4/80 (1:80) (123137, BioLegend, USA), CD11b (1:200) (101206, BioLegend, USA), and CD86 (1:80) (105012. Biolegend, USA).

After sacrificing the mice, the spleen was bluntly dissected and the surface capsule and adipose tissue were discarded. After grinding the tissue sample, red blood cell lysis buffer was added, followed by resuspension and centrifugation. The cell pellet was then treated with a viability dye (1:500) (423101, BioLegend) and blocked with CD16/32 (1:50) (101302, BioLegend). This was followed by staining with mouse CD45 (1:80) (103154, BioLegend, USA), F4/80 (1:80) (123137, BioLegend, USA), CD11b (1:200) (101206, BioLegend, USA), and CD86 (1:80) (105012. Biolegend, USA).

After staining, the cells were washed and resuspended in 1% BSA buffer. Finally, flow cytometry data were collected using a flow cytometer (Attune NxT, Thermo Fisher Scientific) and analyzed using FlowJo software (10.8.1).

In vivo imaging

To elucidate the in vivo distribution of Micro DEA2k in normal and model mice, 1 mL of Cy7-labeled Micro DEA2k (0.4 mg/mL) was injected intraperitoneally into model mice prior to abdominal closure. Normal mice were injected intraperitoneally with 1 mL of Cy7-labeled Micro DEA2k (0.4 mg/mL) as the control group ($n = 3$). After injection, they were monitored with an in vivo imaging system (IVIS Spectrum, PerkinElmer, Inc.), and in vivo imaging was performed at 0, 6, 24, and 48 h. Three additional mice were taken from each group and were sacrificed and dissected at two time points (6 and 24 h). The brain, heart, lungs, liver, kidneys, testes, spleen, and small intestines were excised for ex vivo imaging. To examine the in vivo distribution of Micro DEA2k and DEA2k in the model mice, three additional model mice were injected intraperitoneally with 1 mL of Cy7-labeled DEA2k (0.2 mg/mL). The mice were euthanized and dissected at two time points (6 and 24 h), and the organs were removed for ex vivo imaging.

Statistical analyses

Statistical analysis was performed using GraphPad Prism 9.4.1, and the results were expressed as mean ± SEM. Between-group differences were assessed using the Student's *t*-test (for simple two-sample or paired sample comparisons) or one-way analysis of variance and Tukey's post hoc test (for multiple comparisons). The Kaplan-Meier method was used to compare the differences in survival rates. The Spearman correlation coefficient (R^2) was used to evaluate correlations in the clinical data.

Results

Postoperative abdominal cfDNA levels are elevated in patients after laparoscopic gastrointestinal surgery and are associated with pro-inflammatory cytokines

The physiological structure of the intestinal microvasculature increases the susceptibility to changes in blood flow during pneumoperitoneum, leading to I/R injury [3]. Previous studies have shown that significant elevations in cfDNA levels can be detected in organs such as the myocardium and liver following I/R injury, which can promote an inflammatory response [8, 9, 26]. Therefore, we hypothesized that intestinal I/R injury after laparoscopic surgery leads to cfDNA release and triggers inflammatory dysregulation. First, cfDNA levels in the serum and peritoneal drainage fluid of patients who underwent laparoscopic gastrointestinal surgery were examined immediately and 6 h after surgery. We found that the cfDNA level in the peritoneal drainage fluid of patients was significantly higher at 6 h than immediately after surgery (Fig. 2A); however, no significant elevation was observed in the serum (Fig. 2B). This result may have been obtained because an intraperitoneal drain was placed in all patients after surgery, which decreased the absorption of cfDNA in the peritoneal cavity. Furthermore, correlation analysis showed that the operative duration, as well as the time of the first postoperative flatus, was positively correlated with the cfDNA level in the peritoneal drainage fluid 6 h after surgery (Fig. 2C and Fig. S1). In addition, we measured the serum levels of the inflammatory factors C-reactive protein (CRP), interleukin 6 (IL-6), and procalcitonin (PCT) immediately and 6 h after surgery. Consistent with the changes in cfDNA, the levels of CRP, IL-6, and PCT were significantly higher at 6 h than immediately after surgery (Fig. 2D–F) and were positively correlated with the cfDNA level in the peritoneal drainage fluid at the same time point (Fig. 2G–I). These results suggest that elevated cfDNA levels after intestinal I/R promote the production of inflammatory cytokines and lead to abnormal postoperative intestinal function.

Changes of cfDNA in mouse intestinal I/R injury model

In the present study, we constructed a mouse model of intestinal I/R injury [16, 27]. This process involved clamping the SMA for 45 min and then restoring blood flow (Fig. 3A) [17, 18]. To assess the dynamic changes in cfDNA after I/R injury, peritoneal lavage fluid and serum were collected at 0, 3, 6, 9, 12, and 24 h after reperfusion. Our findings revealed that cfDNA levels in both the peritoneal lavage fluid and serum began to increase at 0 h after reperfusion, peaked at 6 h, and then gradually declined (Fig. 3B, C). Clinical scoring was performed on the mice at each time point, which included assessments of diarrhea, mental status, and elicitation of various reflexes. A higher clinical score was associated with a worse overall condition. Interestingly, the clinical score within 24 h of reperfusion showed a trend similar to that of changes in cfDNA (Fig. 3D). These results suggest that cfDNA levels are elevated in the early stages of I/R injury and may exacerbate the injury.

Synthesis of pH-responsive Micro DEA2k

The working principle of cfDNA scavengers involves the physical binding of the positively charged cationic material to negatively charged cfDNA. Unlike traditional treatments that only address the symptoms of inflammation, cfDNA scavengers mainly target the cause of disease by eliminating agonists that lead to the overexpression of pattern recognition receptors (PRRs). A unique feature of cfDNA scavengers is their ability to reduce the immune response in a dose-dependent manner, effectively eliminating the overactivation of PRRs [28]. However, the potential cytotoxicity of cfDNA scavengers to the human body is a major obstacle to their application. Researchers have attempted to use surface modification methods to reduce the toxicity of cationic materials. Xu et al. developed an siRNA delivery system, PEG-Dlinkm-PLGA, that is stable at the pH of normal tissues and can enhance the cellular uptake of tumor cells by facilitating PEG detachment at the pH of the tumor extracellular microenvironment [29]. However, non-specific protein binding and insufficient targeting must be overcome when designing cfDNA scavengers [30, 31]. Cationic nanomaterials for cfDNA scavenging have been used in animal experiments to treat cfDNA-associated diseases such as periodontitis, sepsis, and rheumatoid arthritis [6, 11, 13]. However, their role in intestinal I/R remains poorly understood.

Considering the issues above, combined with the acidic microenvironment characteristic of inflammation [16], we synthesized innovative phosphorus-responsive cMPs that yielded significant improvements in cytotoxicity, non-specific protein binding, and targeting. Figure 4A shows the preparation process for Micro DEA2k. The proton nuclear magnetic resonance (NMR) spectrum indicated the successful preparation of the pentablock cationic polymer (DEA2k) (Fig. S2A-C), and the GPC elution curve showed a narrow molecular weight distribution (Fig. S2D). Using molecular dynamics

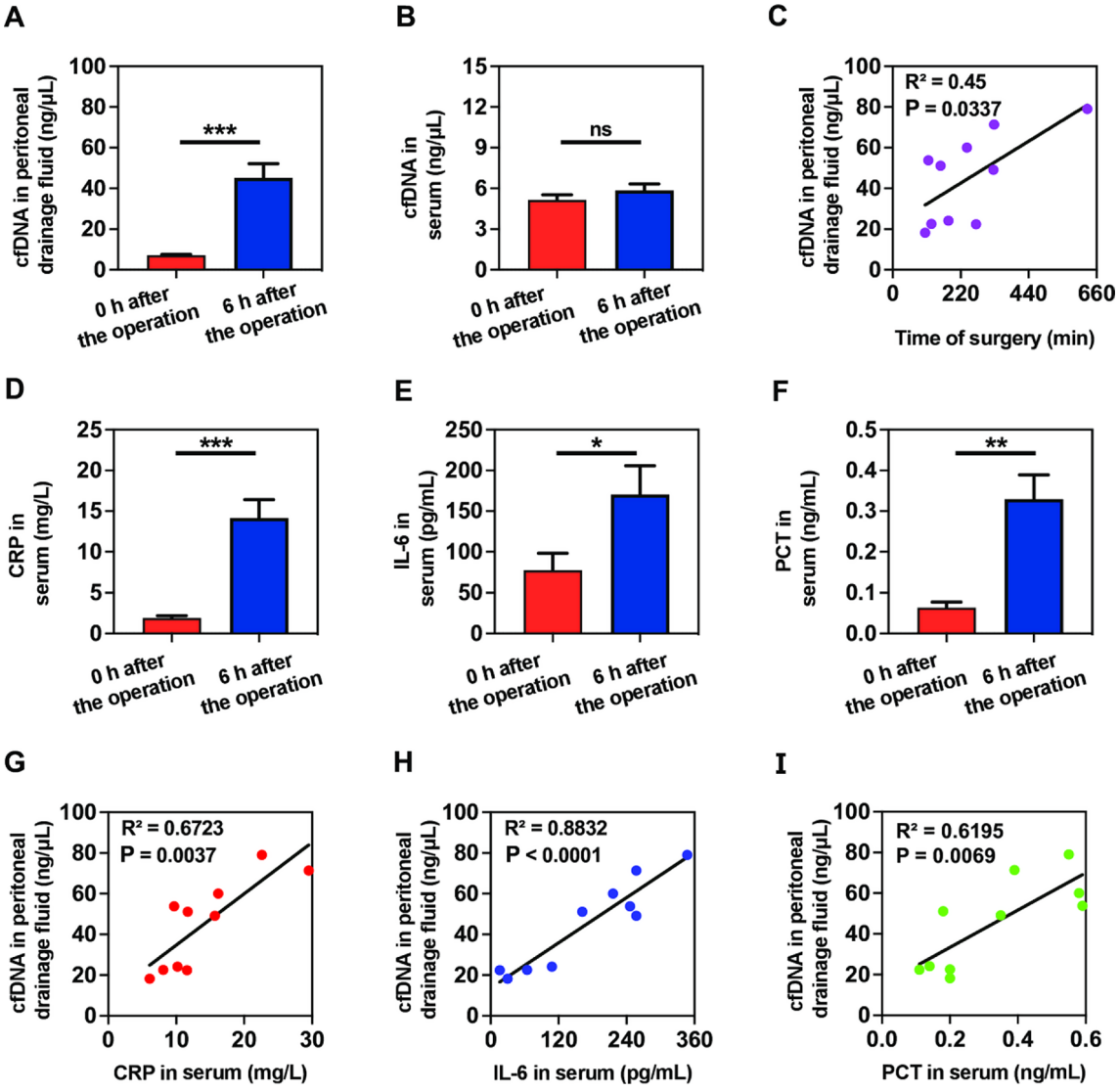

Fig. 2 Strong correlations of postoperative cfDNA levels with operative duration and levels of inflammatory factors in patients after laparoscopic surgery. (**A**) cfDNA levels in peritoneal drainage fluid of patients immediately and 6 h after laparoscopic gastrointestinal surgery. (**B**) Serum cfDNA levels of patients immediately and 6 h after the surgery. (**C**) Positive correlations of cfDNA level in peritoneal drainage fluid at 6 h after the surgery with operative duration. (**D**), (**E**), and (**F**) Serum CRP, IL-6, and PCT levels, respectively, in patients immediately and 6 h after the surgery. (**G**), (**H**), and (**I**) Positive correlations of cfDNA level in peritoneal drainage fluid at 6 h after the surgery with serum CRP, IL-6, and PCT levels, respectively, at 6 h after the surgery. $n = 10$ for each group. Data are expressed as means ± SEM, $^{*}P < 0.05$, $^{**}P < 0.01$, $^{***}P < 0.001$, ns: no significant difference

simulations, four caprolactone repeating units modified by DEA were used to interact with the DNA structure, and 100 repeated molecular docking experiments were performed. The conformation with the lowest binding energy was selected based on the docking results (Fig. 4B, C). Its relevant parameters (Table S1) showed that the binding free energy E_B of the repeating unit segment after tertiary amine protonation was reduced from −7.15 to −8.11 kcal/mol, which demonstrated that the DEA-modified PCL chain had a strong affinity with DNA after tertiary amine protonation. Next, the DEA2k polymer and PCL microspheres were mixed evenly at a mass ratio of 1:1 and centrifuged to obtain cMPs (Micro DEA2k). The DEA2k polymer can self-assemble in an aqueous solution to form nanovesicle structures, as shown by TEM (Fig. S2E). Furthermore, when DEA2k was mixed with PCL microspheres in aqueous solution, DEA2k attached to the surface of the PCL microspheres to form a stable coating layer [32]. Micro DEA2k exhibited a microsphere-like structure under TEM (Fig. S2F). The particle sizes of DEA2k and Micro DEA2k were 183.93 ± 1.59 (nm) and 6201.33 ± 74.27 (nm), respectively, and their polydispersity indices (PDIs) were 0.279, and 0.322, respectively (Fig. 4D). The zeta potentials of DEA2k and Micro DEA2k were 24.76 ± 0.64 and 19.7 ± 1.65 (mV), respectively (Fig. 4E).

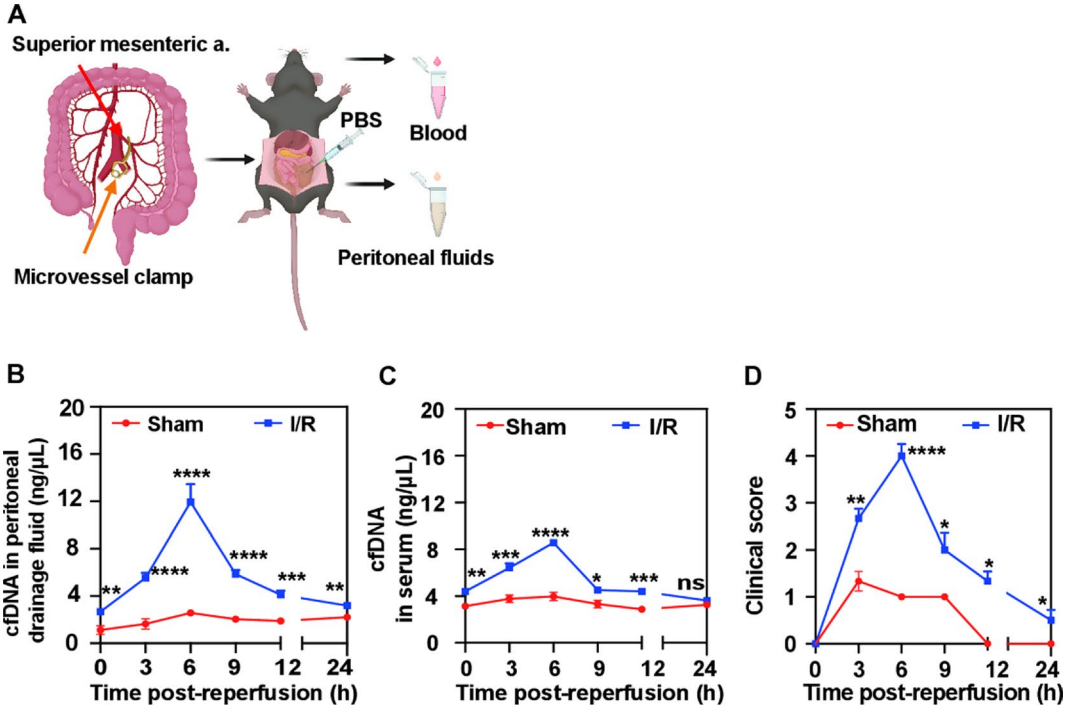

Fig. 3 Trends of cfDNA levels in the intestinal I/R injury model. (**A**) Schematic diagram of the mouse model of intestinal I/R injury. (**B**) and (**C**) Dynamic changes of cfDNA in peritoneal lavage fluid and serum, respectively, at different time points within 24 h after reperfusion. (**D**) Clinical scores at different time points within 24 h after reperfusion. $n = 6$ for each group. Data are expressed as means ± SEM, $^{*}P < 0.05$, $^{**}P < 0.01$, $^{***}P < 0.001$, $^{****}P < 0.0001$, ns: no significant difference

Characterization of DEA2k and Micro DEA2k

The study investigated several characteristics of DEA2k and Micro DEA2k, including toxicity, nucleic acid-binding capacity, chemical stability, and degradation performance. The toxicity of a cationic material directly determines its application prospects; hence, we examined its cytotoxicity. The cytotoxicity of DEA2k and Micro DEA2k at different concentrations was tested on RAW 264.7 cells by the MTT assay (Fig. S3A). The half-maximal inhibitory concentrations (IC50) of DEA2k and Micro DEA2k were then obtained by fitting the logistic equation, yielding values of 1627 and 2691 μg/mL, respectively, thus indicating low cytotoxicity for both. However, the protein adsorption assay revealed that the protein adsorption capacity of Micro DEA2k was significantly lower than that of DEA2k (Fig. S3B). Potentiometric acid-base titration of DEA2k was performed to measure the cumulative amount of sodium hydroxide solution added and the corresponding pH, and the titration curve was plotted (Fig. S4A, B). The buffer capacity of DEA2k, calculated based on the formula, was found to be 2.49 $mmol{\cdot}L^{-1}{\cdot}pH^{-1}$. Because DEA2k has two different amine groups, it must be acidified to a pH of 5–6 to be fully protonated. Therefore, at physiological pH, DEA2k carries a small charge that prevents non-specific binding in the body and reduces its biological toxicity. Like other cationic nanomaterials, DEA2k and Micro DEA2k scavenge cfDNA through the electrostatic attraction between positive and negative charges. Agarose gel electrophoresis was used to detect the nucleic acid-binding capacity of DEA2k and Micro-DEA2k. At a nitrogen-to-phosphorus (N/P) ratio of 4, DEA2k bound to almost all CpGs (Fig. 5A). Similarly, Micro DEA2k bound to almost all CpGs at an N/P ratio of 4 (Fig. 5B). The nucleic acid-binding capacity DEA2k was quantified by fluorescence quenching titration with a nucleic acid dye. As the concentration of DEA2k gradually increased in PBS (pH = 7.4), it with EtBr for binding to calf thymus DNA (ctDNA), resulting in a gradual decrease in the fluorescence emission spectrum (Fig. 5C). This phenomenon was more pronounced in SABS (pH 5.0) (Fig. 5D). The fluorescence quenching reaction parameters (Table S2) calculated from the fluorescence emission spectrum show that the binding constant K_b of DEA2k increased from 6.43 (kM^{-1}) in PBS to 17.9 (kM^{-1}) in SABS. Cationic material can cleave into low molecular weight fragments under acidic conditions, and the degradation process is influenced by factors such as temperature, pH value, time, etc [33]. We simulated the lysosomal acidic environment and physiological body temperature (37 ℃), and used GPC to characterize the degradation process of DEA2k under acidic and physiological temperature conditions. The GPC trace suggested that after 14 days, DEA2k was almost entirely degraded into PEG fragments

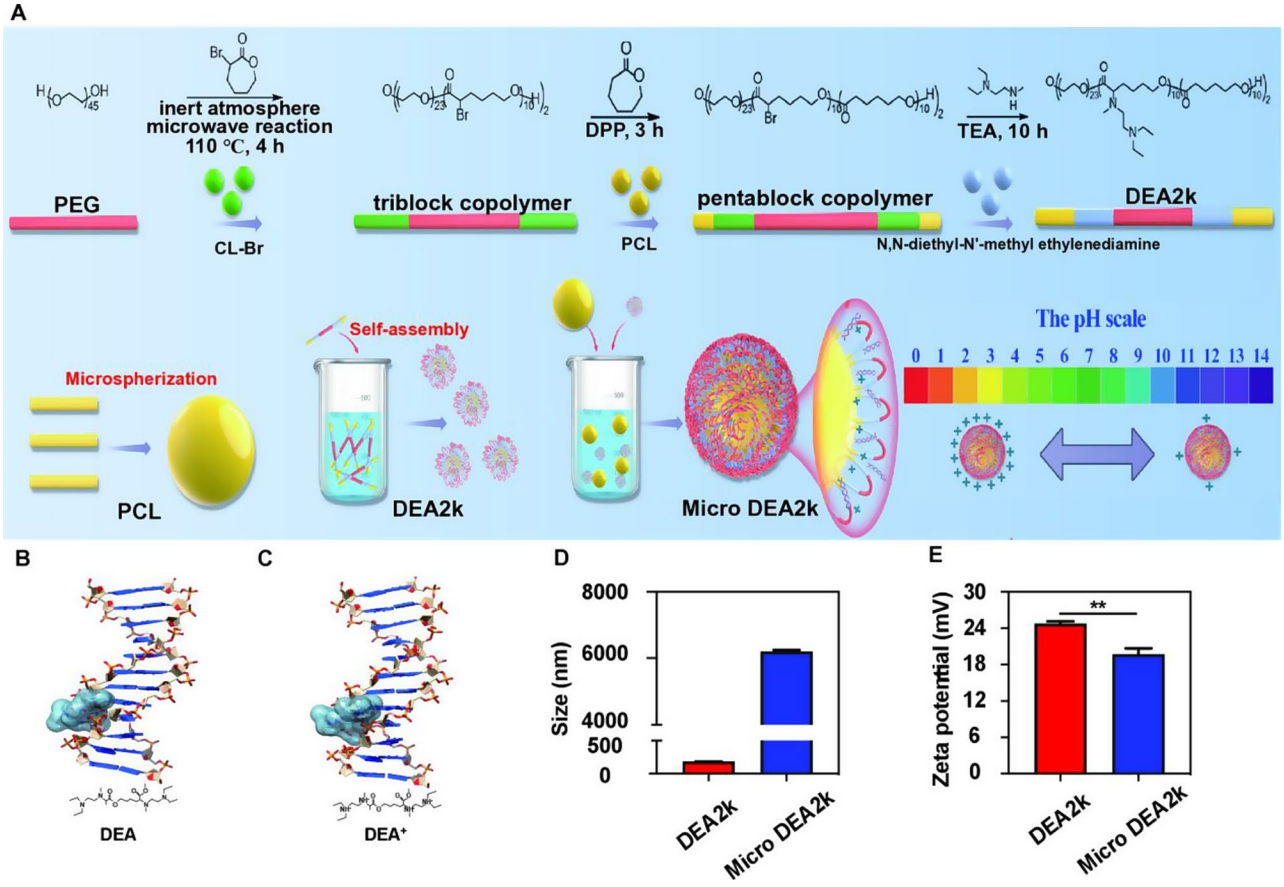

Fig. 4 Synthesis of DEA2k and Micro DEA2k. (**A**) Schematic diagram of the synthesis of DEA2k and Micro DEA2k. (**B**) Side view of the lowest binding pose of the DEA segment after binding to DNA. (**C**) Side view of the lowest binding pose of the protonated DEA segment after binding to DNA. (**D**) and (**E**) Particle sizes and zeta potentials of DEA2k and Micro DEA2k, respectively. $n = 3$ for each group. Data are expressed as means ± SEM, $^{**}P < 0.01$

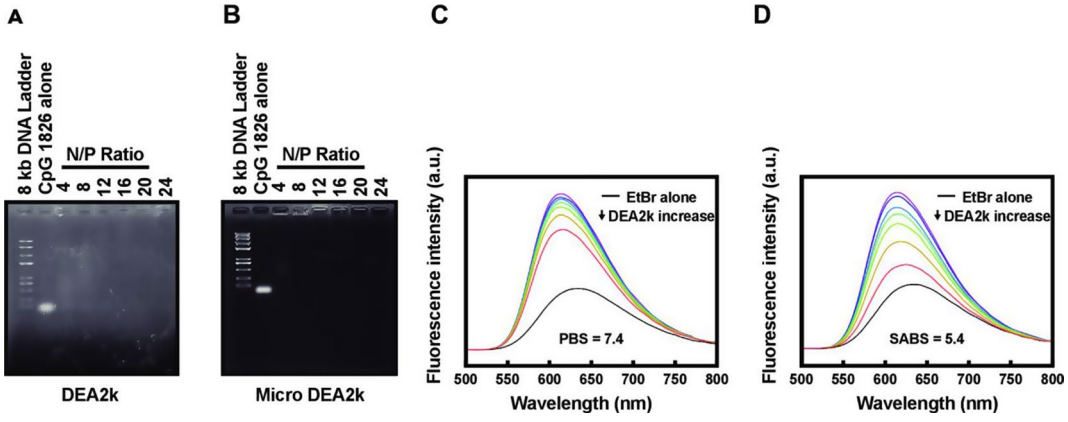

Fig. 5 Measurement of nucleic acid binding capacity. (**A**) Agarose gel electrophoresis image of the DEA2k and CpG1826 complex. (**B**) Agarose gel electrophoresis image of the Micro DEA2k and CpG1826 complex. (**C**) Fluorescence quenching titration emission spectrum of DEA2k in PBS (pH = 7.4). (**D**) Fluorescence quenching titration emission spectrum of DEA2k in SABS (pH = 5.0). The black solid line indicates that only EtBr (1.83 μM) is present in the solution, and the spectrum is elevated to the highest line in the figure after the addition of ctDNA (10.5 μM). The colored lines from top to bottom represent DEA2k at concentrations of 0.33, 0.67, 1, 1.33, 1.67, 2.33, 2.67, and 3.33 μg/mL

under acidic conditions, whereas the effect of temperature on DEA2k degradation was weaker than that of the acidic conditions (Fig. S5 and Table S3). Meanwhile, the stability data of sizes and ζ-potentials were also supplemented in Fig. S6 and Table S4, showing that the sizes and ζ-potentials of both self-assembled DEA2k and Micro DEA2k did not significantly change after 14 days' immersion in PBS at 37 ℃. These results demonstrated

that DEA2k and Micro DEA2k have low cytotoxicity, strong nucleic acid binding capacity which are pH-responsive, and satisfactory chemical stability.

Early use of Micro DEA2k can alleviate the inflammatory response and multi-organ damage caused by intestinal I/R injury

Given that cfDNA levels are elevated in the early stages after I/R injury and can promote the release of inflammatory factors to exacerbate organ damage [11], we administered mice a therapeutic dose of Micro DEA2k via intraperitoneal injection prior to abdominal closure. These mice exhibited significantly higher survival rates after 24 h of I/R (Fig. S7A). As previously described, intraperitoneal injection of Micro DEA2k can significantly reduce the levels of cfDNA, tumor necrosis factors α (TNF-α) and IL-6 (pro-inflammatory factors), and monocyte chemoattractant protein 1 (MCP-1; chemokine) in the peritoneal lavage fluid and serum at 6 h after I/R (Fig. 6A, B). Along with the clearance of cfDNA and alleviation of the inflammatory response, a significant reduction in the clinical score of mice 6 h after I/R was observed (Fig. S8A). In addition, we measured fatty acid-binding protein 2 (FABP2) and lipopolysaccharide (LPS) in the serum and zonula occludens 1 (ZO-1) in tissues to assess intestinal barrier function. ZO-1 is a cytoplasmic protein that connects tight junction proteins to the cytoskeleton and is a marker of barrier integrity [34]. FABP2 as a marker of intestinal mucosal damage [35]. When the intestinal barrier is compromised, the LPS in the intestine is easily absorbed into the bloodstream. The results showed that Micro DEA2k reduced the level of FABP2 in the serum while also stabilizing the expression of ZO-1 in the small intestine and reducing the level of LPS in the serum (Fig. S8A). Additionally, examination of the intestinal tissue samples revealed that after intestinal I/R, the ischemic segments of the intestine appeared dark red, dull, and murky, with dilation and thinning of the intestinal walls and bloody contents visible in the intestinal lumen. In contrast, the intestinal damage was alleviated by the application of Micro DEA2k (Fig. S7B). HE staining of the untreated intestinal I/R mouse model showed severe inflammatory cell infiltration in the ileum, lungs, kidneys, and liver, indicating multiorgan damage. This damage is primarily due to the large amounts of inflammatory factors and toxic intestinal substances that reach adjacent organs through the bloodstream after intestinal I/R injury and impair their functions [36–38]. The use of Micro DEA2k significantly alleviated multiorgan damage (Fig. 6C), thereby lowering the damage score (Fig. S8B). Consistent with the histological changes in the organs, Micro DEA2k significantly reduced serum levels of AST, ALT, BUN, and CRE in serum (Fig. S8C), indicating that Micro DEA2k could mitigate liver and kidney function damage caused by intestinal I/R injury. These results suggest that intraperitoneally injected Micro DEA2k can effectively adsorb cfDNA produced after intestinal I/R injury and reduce the generation of inflammatory factors, thereby alleviating damage to intestinal tissues as well as other major organs.

Biodistribution and low toxicity of Micro DEA2k

To observe the biodistribution of Micro DEA2k in the body, Cy7-labelled Micro DEA2k was injected intraperitoneally into normal and I/R-injured mice. Then, in vivo near-infrared fluorescence imaging was performed at different time points after injection. The fluorescence intensity in the abdomens of both groups gradually decreased over time. However, compared with normal mice, the fluorescence intensity in the model mice remained relatively high 24 h after injection (Fig. S9). In addition, to determine whether a difference existed in the biodistribution of Micro DEA2k and DEA2k in the model mice, different organs were obtained from some mice for ex vivo near-infrared fluorescence imaging at 6 h and 24 h after injection (Fig. 7A-C). We found that the fluorescence intensity of various organs in model mice injected with Micro DEA2k was stronger than that in normal mice at 6 h after injection. This difference may be due to the pH-responsiveness of the material, which rendered the polymer more hydrophilic in the slightly acidic inflammatory environment of the model mice, leading to stronger diffusivity. The material was predominantly distributed in the small intestine, lungs, testes, spleen, liver, and kidneys, indicating that Micro DEA2k accumulated in these organs (Fig. 7B). Furthermore, the fluorescence intensity of Micro DEA2k was higher than that of DEA2k in the small intestine of I/R mice 6 h after injection, suggesting a longer residence time (Fig. 7A, B). Ex vivo near-infrared fluorescence imaging 24 h after the injection showed a significant decrease in fluorescence intensity in various organs, except the liver (Fig. 7C), suggesting that the cationic material can also be gradually metabolized and cleared by the body as inflammation slowly subsides.

As toxicity is a major concern in the clinical application of cationic materials, we administered healthy mice with an intraperitoneal injection of Micro DEA2k at a 5-fold dose (2 mg/mL), and the mice were observed for 7 d. No decrease in body weight and no significant differences in AST, ALT, CRE, or BUN were observed in the serum of the mice in the Micro DEA2k group compared to that of the mice injected with an equal volume of PBS (Fig. S10A, B). No abnormal pathomorphological changes were observed in the major organs in either group (Fig. S10C). Therefore, Micro DEA2k shows no toxic side effects and is safe for clinical applications.

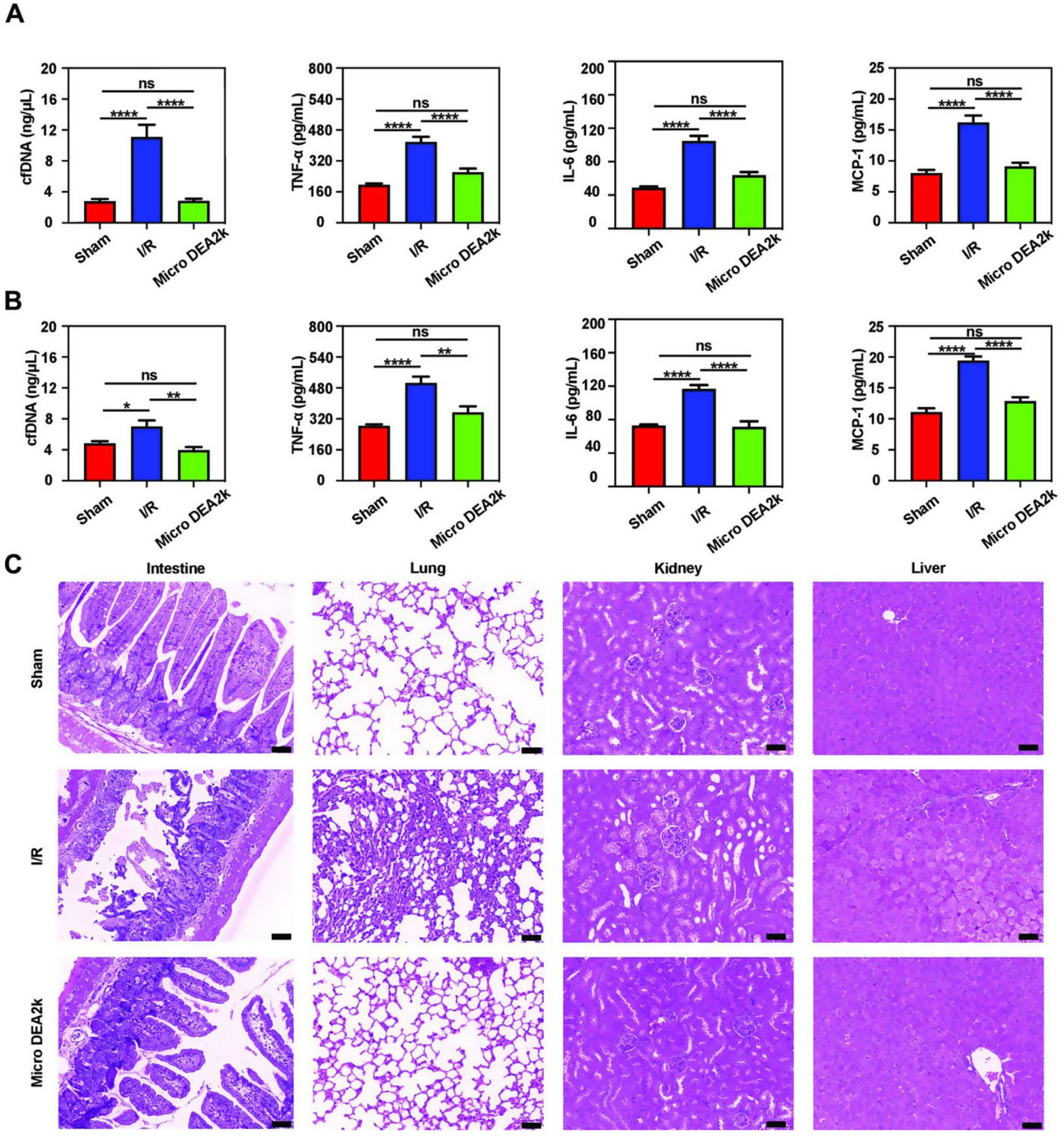

Fig. 6 Micro DEA2k protects mice from inflammatory responses induced by intestinal I/R. (**A**) Levels of cfDNA, TNF-α, IL-6, and MCP-1 in peritoneal drainage fluid at 6 h after reperfusion. (**B**) Levels of cfDNA, TNF-α, IL-6, and MCP-1 in serum at 6 h after reperfusion. (**C**) HE staining of small intestine, lung, kidney, and liver tissues at 6 h after reperfusion, scale bar = 50 μm. $n = 6$ for each group. Data are expressed as means ± SEM, $^{*}P < 0.05$, $^{**}P < 0.01$, $^{***}P < 0.001$, $^{****}P < 0.0001$, ns: no significant difference

Binding of Micro DEA2k to cfDNA inhibits macrophage M1 polarization and alleviates inflammatory response

Following intestinal I/R injury, immune cells such as macrophages will infiltrate the intestinal tissues, whereas cfDNA can activate macrophage TLR9 receptors to induce the transition to the M1 phenotype and release large amounts of pro-inflammatory cytokines such as TNF-α and IL-6 [7, 39]. The TLR9-MyD88-NF-κB signaling pathway is an important signaling pathway for cfDNA-induced macrophage M1 polarization [40, 41]. Therefore, we explored the effects of Micro DEA2k on the macrophage phenotype and inflammatory cytokines

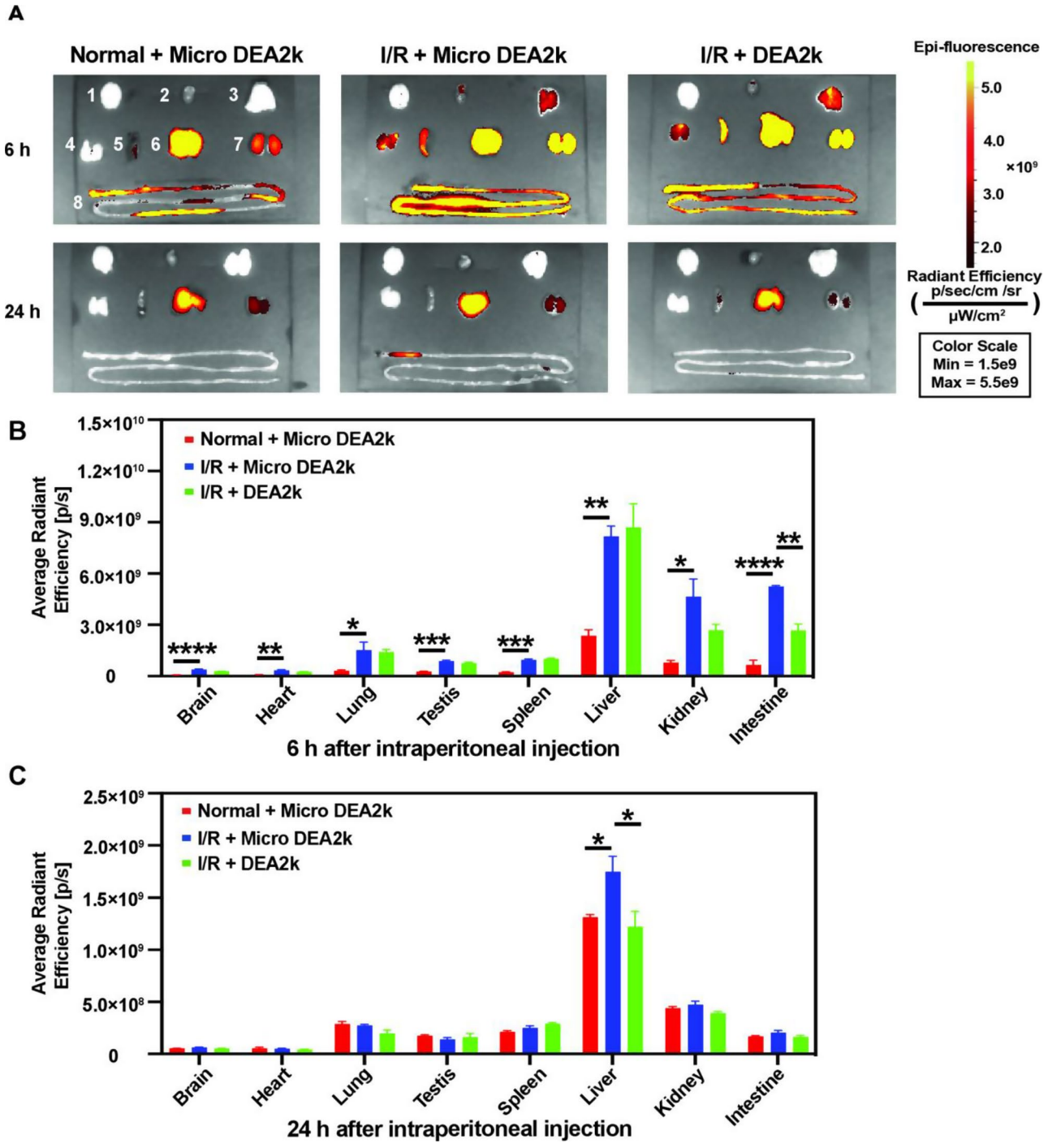

Fig. 7 Biodistribution of Micro DEA2k. (**A**) Ex vivo near-infrared fluorescence imaging of organs in each group at 6 and 24 h after intraperitoneal injection of Cy7-labeled Micro DEA2k or DEA2k. Figure legend: (1) Brain; (2) Heart; (3) Lung; (4) Testis; (5) Spleen; (6) Liver; (7) Kidney; (8) Small intestine. (**B**) Semi-quantitative analysis of each organ by in vivo near-infrared fluorescence imaging at 6 h after the injection. (**C**) Semi-quantitative analysis of each organ by in vivo near-infrared fluorescence imaging at 24 h after the injection. $n = 3$ for each group. Data are expressed as means ± SEM, $^{*}P < 0.05$, $^{**}P < 0.01$, $^{***}P < 0.001$, $^{****}P < 0.0001$

through in vivo and ex vivo experiments. In the ex vivo experiment, RAW 264.7 cells were stimulated and activated with FAM-labeled CpG (FAM-CpG), followed by localization and characterization using fluorescence microscopy. When no Micro DEA2k was added, CpG was dispersed in the lysosomes (Fig. 8A, as indicated by the red arrow). When Micro DEA2k was added, although the fluorescence intensity of intracellular CpG did not

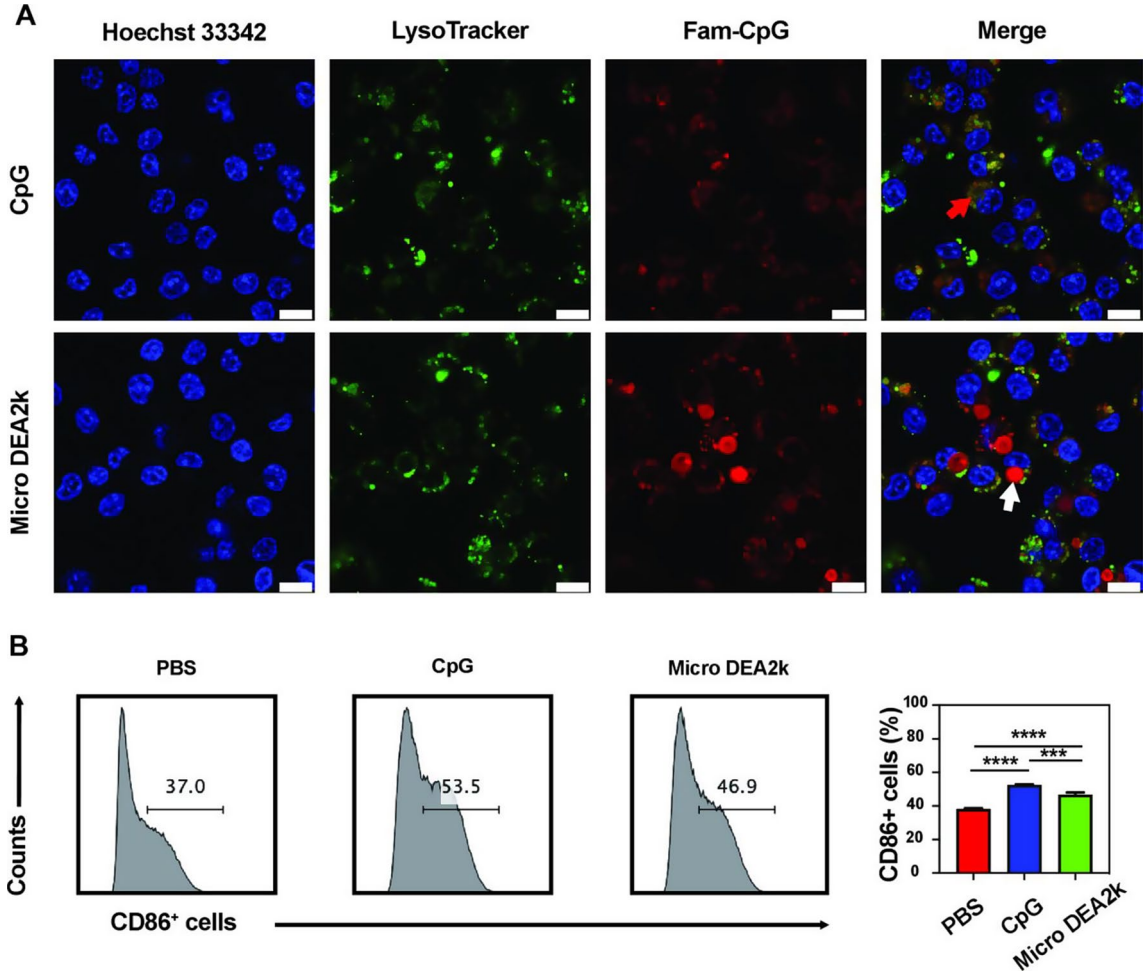

Fig. 8 Micro DEA2k can bind with cfDNA in vitro to reduce the number of M1 macrophages. (**A**) Intracellular localization of CpG and Micro DEA2k in RAW 264.7 macrophages after 24 h of co-incubation, scale bar = 10 μm; the red arrows indicate the intracellular localization of CpG in the absence of Micro DEA2k, and the white arrows indicate the intracellular localization of CpG after the addition of Micro DEA2k. (**B**) Proportion of M1 cells in RAW 264.7 macrophages. (**C**) Mechanism of action of Micro DEA2k. $n = 6$ for each group. Data are expressed as means ± SEM, $^{***}P < 0.001$, $^{****}P < 0.0001$

decrease, CpG was distributed in a circular and centralized manner within the lysosomes (Fig. 8A, as indicated by the white arrow). The results show that cfDNA primarily accumulates in the lysosomes of macrophages, consistent with previous studies [13, 42]. Importantly, the binding site of Micro DEA2k to cfDNA is also within the lysosomes of macrophages. This phenomenon is related to the cellular uptake and metabolic pathways of cationic particles. Typically, cationic particles interact with negatively charged proteoglycans on the cell membrane and are internalized through non-specific endocytosis, with lysosomes serving as the final site for cationic particles metabolism [43]. Consequently, Micro DEA2k adsorbs substantial amounts of cfDNA within lysosomes, thereby inhibiting its binding to TLR9. Notably, the adsorption capacity of Micro DEA2k for cfDNA is maximized under the acidic conditions of lysosomes. Next, the flow cytometry assay (Fig. S11A) revealed that the number of CpG-stimulated pro-inflammatory M1 macrophages was significantly reduced after the application of Micro DEA2k (Fig. 8B). In addition, the expression levels of TNF-α and IL-6 also decreased accordingly (Fig. S11B). Furthermore, we examined the protein expression of TLR9, MyD88, p65, and pp65 and found that their expression was reduced in the Micro DEA2k group (Fig. S11C). This evidence suggests that the in vitro anti-inflammatory mechanism of Micro DEA2k may involve its enhanced ability to bind cfDNA because of the decreased pH after entering the lysosome. By reducing the transduction of the TLR9-MyD88-NF-κB signaling pathway, Micro DEA2k can inhibit the polarization of M1 macrophages and reduce the release of pro-inflammatory factors, thereby exerting a protective effect.

In the in vivo experiment, immunohistochemical analysis was performed on the expression of F4/80 protein, which is a marker for macrophages, in small intestinal tissues. Intraperitoneal injection of Micro DEA2k significantly reduced the F4/80 content (Fig. 9A). The number

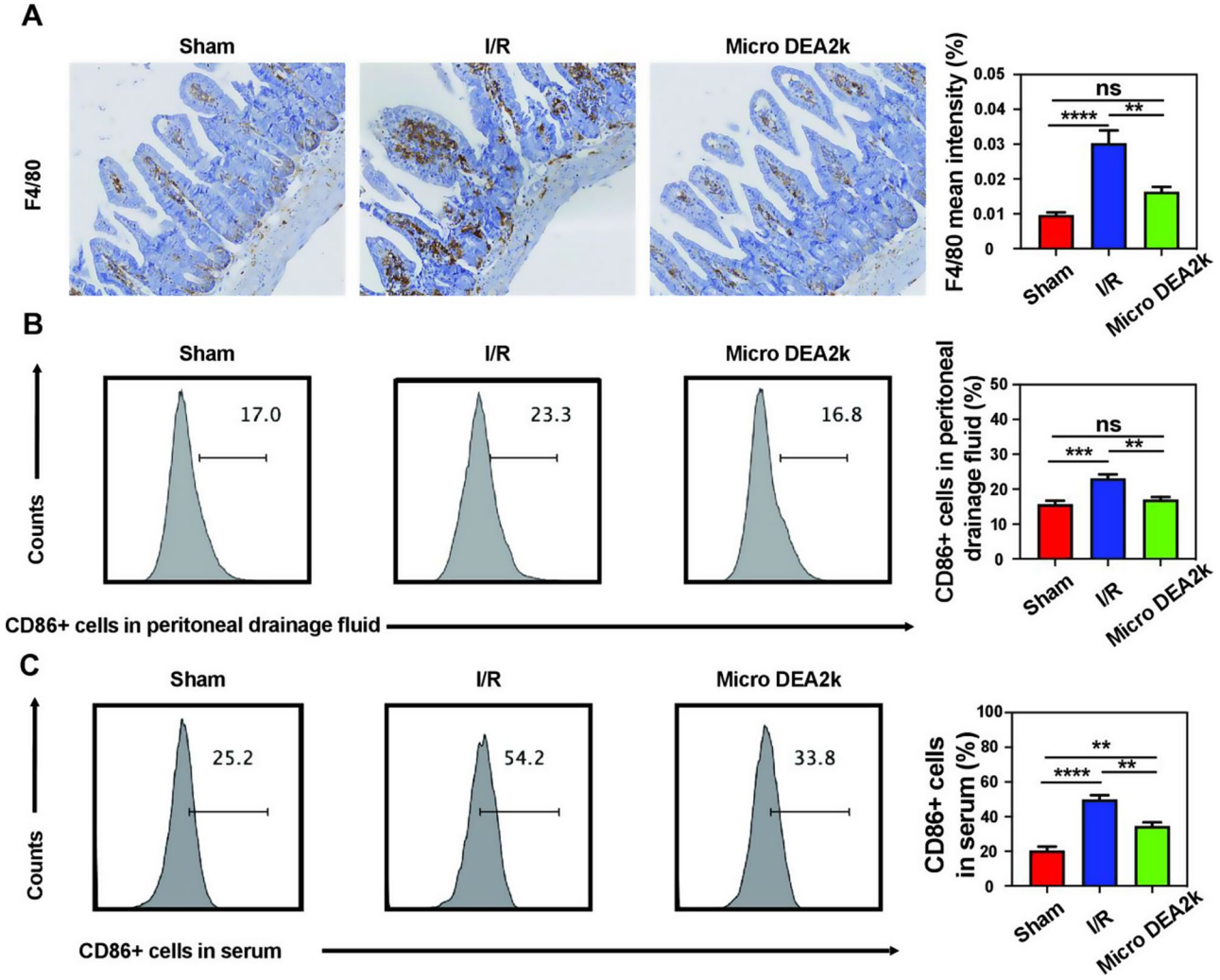

Fig. 9 Micro DEA2k reduces intestinal macrophage infiltration and decreases the number of M1 macrophages in the peritoneal cavity and blood. (**A**) Immunohistochemistry and quantification of small intestinal F4/80, scale bar = 50 μm. (**B**) Proportion of peritoneal CD68 + M1 macrophages. (**C**) Proportion of circulating CD68 + M1 macrophages. $n = 6$ for each group. Data are expressed as means ± SEM, $^{**}P < 0.01$, $^{***}P < 0.001$, $^{****}P < 0.0001$

of CD86-labeled M1 macrophages in the peritoneal lavage fluid and peripheral blood was examined using flow cytometry (Fig. S12). Consistent with the ex vivo cell experiment, Micro DEA2k decreased the number of M1 macrophages in the peritoneal lavage fluid and serum (Fig. 9B, C). Immunohistochemical assays of the small intestinal tissues also revealed a decrease in the relative protein levels of TLR9, MyD88, and p65 (Fig. S13). This finding further demonstrates that Micro DEA2k exerts an anti-inflammatory effect by reducing the activation of the TLR9-MyD88-NF-κB signaling pathway. The above results suggest that intraperitoneally injected Micro DEA2k can adsorb the excessive cfDNA produced after intestinal I/R injury and prevent the overactivation of the TLR9-MyD88-NF-κB signaling pathway, thereby inhibiting the polarization of M1 macrophages and exerting an anti-inflammatory effect.

Discussion

The treatment of intestinal I/R injury remains challenging in clinical practice, with high morbidity and mortality rates. This condition encompasses a multitude of pathological processes, including oxidative stress, calcium overload, and inflammatory responses, ultimately leading to the death of intestinal epithelial cells [1, 44, 45]. Subsequently, the release of DAMPs from dying cells activates pro-inflammatory responses in immune cells, such as macrophages, leading to inflammatory dysregulation and exacerbating damage to intestinal and extraintestinal tissues [7]. Consequently, effective management of excessive inflammatory responses is paramount for mitigating the detrimental effects of intestinal I/R injury.

With the increasing elucidation of the role of cfDNA in the pathophysiology of various inflammatory diseases, its involvement in intestinal I/R injury has garnered significant attention [7, 12–14]. A previous study demonstrated

that serum cfDNA levels markedly increase in the early stages following acute mesenteric ischemia in rats, positively correlating with the severity of pathological ischemia [46]. Similarly, our study demonstrated that peritoneal cfDNA levels were significantly elevated and positively correlated with serum inflammatory factors such as CRP, IL-6, and PCT after laparoscopic gastrointestinal surgery. Furthermore, in a mouse model of intestinal I/R injury, cfDNA levels were elevated in the early stages of I/R injury, accompanied by an increase in the clinical score. These findings further suggest that cfDNA and inflammatory responses create a mutually reinforcing positive feedback loop, collectively exacerbating initial organ injury and subsequently initiating a vicious cycle of increased cfDNA, inflammation, and organ damage.

Dysregulation of inflammation mediated by cfDNA primarily stems from the activation of inflammatory signaling pathways within immune cells, with macrophages serving as pivotal effector cells. Macrophages have been extensively studied as innate immune cells owing to their contribution to organ I/R injury, and their functional characteristics are governed by their distinct phenotypic states [47]. Macrophages are primarily categorized into two distinct phenotypes, M1 and M2. M1 macrophages exhibit a proinflammatory phenotype characterized by the robust release of pro-inflammatory cytokines and chemokines, thereby playing a pivotal role in mediating inflammatory dysregulation. In contrast, M2 macrophages display anti-inflammatory and repair-oriented phenotypes, inhibiting inflammation and facilitating tissue repair. In animal models of intestinal I/R injury, significant infiltration of M1 macrophages has been documented in intestinal tissues, and an elevation in cfDNA levels has been shown to stimulate the polarization of macrophages towards the M1 phenotype [48]. To counteract this effect, Wang et al. administered deoxyribonuclease I (DNase-1) intravenously to degrade cfDNA. This approach significantly alleviated intestinal inflammation following intestinal I/R injury in rats, restored intestinal barrier integrity, and enhanced the expression of tight junction proteins [11]. Consequently, clearance or neutralization of cfDNA is a vital anti-inflammatory strategy for mitigating intestinal I/R injury.

Nucleic acid scavengers (NAS) have been developed for various disease models; however, several unresolved issues persist concerning their cytotoxicity, biocompatibility, biodegradability, and in vivo biodistribution. To mitigate the limitations associated with NAS, various safer alternatives and modification strategies have been explored and reported. Additionally, NAS can be integrated with hydrogels or electrospun fibers to achieve multifunctional therapeutic effects. Overall, NAS can be tailored or modified in a personalized manner based on disease models, routes of administration, and functional requirements to optimize their therapeutic efficacy. Table S5 provides a summary of the NAS reported in recent years. Given that low pH is a pivotal characteristic of the inflammatory microenvironment [16], we devised cationic nanoparticles (DEA2k) that undergo substantial protonation of tertiary amines solely within a pH range of 5–6. This implies that under normal microenvironments, DEA2k exhibits minimal protonation, displaying a weak positive charge, thus reducing its impact on other cells and manifesting low cytotoxicity. However, our administration route was via intraperitoneal injection, where cationic materials are absorbed through the peritoneal and omental blood vessels and subsequently enter the liver via the superior mesenteric and hepatic portal veins. At this point, Kupffer cells residing in the liver capture the majority of nanomedicines or nanoparticles, significantly reducing their residence time in the body, thereby affecting the clearance efficiency of cfDNA [49]. Notably, Aneta Cymbaluk-Płoska and colleagues discovered that microcapsules loaded with carboplatin, with diameters ranging from 10 to 25 μm, could diminish phagocytosis and peritoneal clearance through lymphocyte transport, thereby enabling sustained intraperitoneal release of carboplatin for the treatment of ovarian cancer [50]. Inspired by this pioneering research, we sought to augment the particle size by harnessing the amphiphilic properties of PCEC, combined with PCL as the core, to self-assemble DEA2k into microspherical particles (termed Micro DEA2k), thus scaling them to the micrometer range. Our objective was to investigate whether this enhancement could prolong the residence time within the peritoneal cavity and ultimately enhance the capacity to locally bind cell-free DNA (cfDNA). In vivo imaging results revealed that the intestinal fluorescence intensity was maintained at a relatively high level six hours post-reperfusion following the intraperitoneal injection of Micro DEA2k. Furthermore, Micro DEA2k exhibited reduced protein binding affinity compared to DEA2k. Upon absorption into the bloodstream, it is less prone to forming a protein corona with opsonin proteins, rendering it less susceptible to clearance by mononuclear phagocytes. Consequently, Micro DEA2k demonstrated superior ability to bind cfDNA in circulation. Our experimental results show that we have successfully developed cationic microsphere particles characterized by low toxicity, minimal nonspecific protein-binding rates, and extended intraperitoneal residence times, making them promising candidates for the clearance of cfDNA.

In animal models, we observed that intraperitoneal injection of Micro DEA2k significantly decreased cfDNA levels in both the peritoneal cavity and serum 6 h post-reperfusion. Furthermore, it also reduced the concentrations of inflammatory cytokines IL-6 and TNF-α, as

well as the chemokine MCP-1, in both compartments. Through a combination of in vivo and in vitro experiments, we validated that the TLR9/MyD88/NF-κB signaling pathway in macrophages is a pivotal signaling mechanism underlying cfDNA-mediated inflammation, which exacerbates organ damage. The application of Micro DEA2k inhibited this signaling pathway, thereby suppressing M1 polarization of macrophages and reducing the release of inflammatory cytokines such as IL-6 and TNF-α. Consequently, it improves the survival rate of mice subjected to intestinal I/R injury. Additionally, by clearing cfDNA, Micro DEA2k stabilizes the expression of intestinal ZO-1 protein, maintains the integrity of the intestinal barrier, decreases LPS absorption into the bloodstream, and alleviates damage to other distant organs.

Conclusion

In summary, this study elucidates the crucial role of cfDNA in intestinal I/R injury. The pH-responsive cMPs Micro DEA2k developed in this study improved the survival rate and reduced multiorgan damage by inhibiting the polarization of M1 macrophages after intestinal I/R injury and alleviating local and systemic inflammatory responses. This study presents a feasible method for cfDNA clearance that is safe, effective, and promising for clinical applications.

Supplementary Information

The online version contains supplementary material available at https://doi.org/10.1186/s12951-025-03231-2.

Supplementary Material 1

Author contributions

Hanbin Xie: Writing– original draft, Methodology, Investigation, Formal analysis, Project administration. Cong Wei: Investigation, Methodology, Project administration, Writing– review & editing. Chang Xiong: Investigation, Methodology, Project administration. Ziyan Huang: Investigation, Methodology, Project administration. Chaojin Chen: Methodology. Xue Xiao: Methodology. Linan Zhang: Software, Visualization. Zhenjia Lin: Resources, Visualization. Ziqing Hei: Conceptualization, Methodology, Investigation, Validation, Visualization, Writing– review & editing, Funding acquisition, Project administration, Resources, Supervision. Tianyu Zhao: Conceptualization, Methodology, Investigation, Validation, Visualization, Writing–review & editing, Project administration, Resources, Supervision. Weifeng Yao: Conceptualization, Methodology, Visualization, Writing– review & editing, Funding acquisition, Project administration, Resources, Supervision. All authors reviewed the manuscript.

Funding

This study was supported by several grants from the Joint Funds of the National Natural Science Foundation of China (grant no. U22A20276), National Natural Science Foundation of China (grant nos. 82472217, 81974296, and 52103276), National Key Research and Development Program of China (grant no. 2022YFC2304200), Guangdong Provincial Natural Science Foundation, Provincial-Enterprise Joint Project (grant nos. 2024A1515220097), Guangdong Basic and Applied Basic Research Foundation (grant nos. 2021B1515230012, 2021A1515012318, and 2022A1515010947), "Five and five" Project of the Third Affiliated Hospital of Sun Yat-sen University (grant no. 2023WW501), Science and Technology Planning Project of Guangdong Province (grant no. 2023B110006), Key Areas Research and Development Program of Guangzhou (grant no. 202007020006), Science and Technology Program of Guangzhou (grant nos. 202102010190, 202201010765, 202201020429, 202201011343, and 202201020261), and Fundamental Research Funds for the Central Universities, Sun Yat-sen University (grant nos. 23ykbj004 and 23qnpy03).

Data availability

No datasets were generated or analysed during the current study.

Declarations

Ethics approval and consent to participate

All experiments involving human tissues were conducted in accordance with the Helsinki criteria and approved by the Ethics Committees of the Third Affiliated Hospital of Sun Yat-sen University. All experiments involving mice were conducted in accordance with protocols approved by the Animal Ethics Committee of South China Agricultural University.

Consent for publication

This work has not been published previously and is not under consideration for publication elsewhere. Its publication is approved by all the authors and tacitly or explicitly by the responsible authorities where the work was carried out; if accepted, it will not be published elsewhere in the same form, in English or any other language, including electronically, without the written consent of the copyright holder.

Competing interests

The authors declare no competing interests.

Author details

[1]Department of Anesthesiology, The Third Affiliated Hospital of Sun Yat-Sen University, Guangzhou, Guangdong 510635, China
[2]School of Materials Science and Engineering, Sun Yat-Sen University, Guangzhou, Guangdong 510275, China
[3]Guangdong Cardiovascular Institute, Guangdong Provincial People's Hospital, Guangdong Academy of Medical Sciences, Guangzhou, Guangdong 510080, China
[4]Zhaoqing Campus of the Third Affiliated Hospital of Sun Yat Sen University, Zhaoqing, Guangdong 526000, China

Received: 14 December 2024 / Accepted: 11 February 2025
Published online: 28 February 2025

References

1. Lenaerts K, Ceulemans LJ, Hundscheid IH, et al. New insights in intestinal ischemia-reperfusion injury: implications for intestinal transplantation. Curr Opin Organ Transpl. 2013;18(3):298–303.
2. Kong C, Song W, Ren J, et al. Circulating mtDNA and impaired intestinal barrier after gastrointestinal surgery are correlated with postoperative SIRS. Genes (Basel). 2022;13(11):1933.
3. Papparella A, Nino F, Coppola S, et al. Peritoneal morphological changes due to pneumoperitoneum: the effect of intra-abdominal pressure. Eur J Pediatr Surg. 2014;24(4):322–7.
4. Zhang X, Wu J, Liu Q, et al. mtDNA-STING pathway promotes necroptosis-dependent enterocyte injury in intestinal ischemia reperfusion. Cell Death Dis. 2020;11(12):1050.
5. Arifa RDN, de Paula TP, Lima RL, et al. Anti-inflammatory and antioxidant effects of the nanocomposite Fullerol decrease the severity of intestinal inflammation induced by gut ischemia and reperfusion. Eur J Pharmacol. 2021;898:173984.
6. Deitch EA, Xu D, Kaise VL. Role of the gut in the development of injury- and shock induced SIRS and MODS: the gut-lymph hypothesis, a review. Front Biosci. 2006;11:520–8.
7. Cheng F, Su T, Liu Y, et al. Targeting lymph nodes for systemic immunosuppression using cell-Free-DNA-Scavenging and cGAS-Inhibiting Nanomedicine-In-Hydrogel for rheumatoid arthritis immunotherapy. Adv Sci (Weinh). 2023;10(26):e2302575.
8. Schütz E, Fischer A, Beck J, et al. Graft-derived cell-free DNA, a noninvasive early rejection and graft damage marker in liver transplantation:

a prospective, observational, multicenter cohort study. PLoS Med. 2017;14(4):e1002286.
9. Tian Y, Charles EJ, Yan Z, et al. The myocardial infarct-exacerbating effect of cell-free DNA is mediated by the high-mobility group box 1-receptor for advanced glycation end products-toll-like receptor 9 pathway. J Thorac Cardiovasc Surg. 2019;157(6):2256–69.
10. Huang W, Wen L, Tian H, et al. Self-propelled proteomotors with active cell-free mtDNA clearance for enhanced therapy of Sepsis-Associated Acute Lung Injury. Adv Sci (Weinh). 2023;10(27):e2301635.
11. Wang S, Xie T, Sun S, et al. DNase-1 treatment exerts protective effects in a rat model of Intestinal Ischemia-Reperfusion Injury. Sci Rep. 2018;8(1):17788.
12. Dawulieti J, Sun M, Zhao Y, et al. Treatment of severe sepsis with nanoparticulate cell-free DNA scavengers. Sci Adv. 2020;6(22):eaay7148.
13. Huang H, Pan W, Wang Y, et al. Nanoparticulate cell-free DNA scavenger for treating inflammatory bone loss in periodontitis. Nat Commun. 2022;13(1):5925.
14. Wu K, Lu X, Li Y, et al. Polyglycerol-amine covered Nanosheets Target Cell-Free DNA to Attenuate Acute kidney Injury. Adv Sci (Weinh). 2023;10(23):e2300604.
15. Liu F, Sheng S, Shao D, et al. A Cationic Metal-Organic Framework to scavenge cell-free DNA for severe Sepsis Management. Nano Lett. 2021;21(6):2461–9.
16. Wong CW, Pratiwi FW, Chen P, et al. Revealing the phagosomal pH regulation and inflammation of macrophages after endocytosing polyurethane nanoparticles by a ratiometric pH Nanosensor. Adv Biol (Weinh). 2021;5(1):e2000200.
17. Wang Z, Sun R, Wang G, et al. SIRT3-mediated deacetylation of PRDX3 alleviates mitochondrial oxidative damage and apoptosis induced by intestinal ischemia/reperfusion injury. Redox Biol. 2020;28:101343.
18. Hayase N, Doi K, Hiruma T, et al. Recombinant thrombomodulin on Neutrophil Extracellular traps in murine intestinal ischemia-reperfusion. Anesthesiology. 2019;131(4):866–82.
19. Spence S, Greene MK, Fay F, Hams E, et al. Targeting siglecs with a sialic acid-decorated nanoparticle abrogates inflammation. Sci Transl Med. 2015;7(303):303ra140.
20. Drew HR, Wing RM, Takano T, et al. Structure of a B-DNA dodecamer: conformation and dynamics. Proc Natl Acad Sci U S A. 1981;78(4):2179–83.
21. Hao J, Kos P, Zhou K, et al. Rapid Synthesis of a Lipocationic Polyester Library via Ring-opening polymerization of functional valerolactones for efficacious siRNA delivery. J Am Chem Soc. 2015;137(29):9206–9.
22. Liu WF, Wen SH, Zhan JH, et al. Treatment with recombinant trichinella spiralis cathepsin B-like protein ameliorates intestinal Ischemia/Reperfusion Injury in mice by promoting a switch from M1 to M2 macrophages. J Immunol. 2015;195(1):317–28.
23. D'Alessio FR, Tsushima K, Aggarwal NR, et al. CD4 + CD25 + Foxp3 + tregs resolve experimental lung injury in mice and are present in humans with acute lung injury. J Clin Invest. 2009;119(10):2898–913.
24. Gu J, Sun P, Zhao H, et al. Dexmedetomidine provides renoprotection against ischemia-reperfusion injury in mice. Crit Care. 2011;15(3):R153.
25. Shen XD, Ke B, Zhai Y, et al. Toll-like receptor and heme oxygenase-1 signaling in hepatic ischemia/reperfusion injury. Am J Transpl. 2005;5(8):1793–800.
26. Xie D, Guo H, Li M, et al. Splenic monocytes mediate inflammatory response and exacerbate myocardial ischemia/reperfusion injury in a mitochondrial cell-free DNA-TLR9-NLRP3-dependent fashion. Basic Res Cardiol. 2023;118(1):44.
27. Deng F, Lin ZB, Sun QS, et al. The role of intestinal microbiota and its metabolites in intestinal and extraintestinal organ injury induced by intestinal ischemia reperfusion injury. Int J Biol Sci. 2022;18(10):3981–92.
28. Bhansali D, Akinade T, Li T, et al. Comparative analysis of nucleic acid-binding polymers as potential anti-inflammatory nanocarriers. Pharmaceutics. 2023;16(1):10.
29. Xu CF, Zhang HB, Sun CY, et al. Tumor acidity-sensitive linkage-bridged block copolymer for therapeutic siRNA delivery. Biomaterials. 2016;88:48–59.
30. Shi T, Zhao J, Long K, et al. Cationic mesoporous silica nanoparticles alleviate osteoarthritis by targeting multiple inflammatory mediators. Biomaterials. 2023;303:122366.
31. Shi C, Dawulieti J, Shi F, et al. A nanoparticulate dual scavenger for targeted therapy of inflammatory bowel disease. Sci Adv. 2022;8(4):eabj2372.
32. Zhong H, Li Z, Zhao T, et al. Surface modification of nanofibers by physical adsorption of Fiber-homologous amphiphilic copolymers and Nanofiber-Reinforced hydrogels with excellent tissue adhesion. ACS Biomater Sci Eng. 2021;7(10):4828–37.
33. Bartnikowski M, Dargaville TR, Ivanovski, et al. Degradation mechanisms of polycaprolactone in the context of chemistry, geometry and environment. Prog Polym Sci. 2019;96:1–20.
34. Wells JM, Brummer RJ, Derrien M, et al. Homeostasis of the gut barrier and potential biomarkers. Am J Physiol Gastrointest Liver Physiol. 2017;312(3):G171–93.
35. van Wijck K, Lenaerts K, Grootjans J, et al. Physiology and pathophysiology of splanchnic hypoperfusion and intestinal injury during exercise: strategies for evaluation and prevention. Am J Physiol Gastrointest Liver Physiol. 2012;303(2):G155–68.
36. Lee J, Lee J, Kim K, et al. Antibiotic-induced intestinal microbiota depletion can attenuate the acute kidney injury to chronic kidney disease transition via NADPH oxidase 2 and trimethylamine-N-oxide inhibition. Kidney Int. 2024;105(6):1239–53.
37. Li Y, Cao Y, Xiao J, et al. Inhibitor of apoptosis-stimulating protein of p53 inhibits ferroptosis and alleviates intestinal ischemia/reperfusion-induced acute lung injury. Cell Death Differ. 2020;27(9):2635–50.
38. Wen S, Li X, Ling Y, et al. HMGB1-associated necroptosis and kupffer cells M1 polarization underlies remote liver injury induced by intestinal ischemia/reperfusion in rats. FASEB J. 2020;34(3):4384–402.
39. Gao Y, Zhang H, Wang Y, et al. L-Cysteine alleviates Myenteric Neuron Injury Induced by Intestinal Ischemia/Reperfusion via Inhibitin the Macrophage NLRP3-IL-1β pathway. Front Pharmacol. 2022;13:899169.
40. Takeuchi O, Akira S. Pattern recognition receptors and inflammation. Cell. 2010;140(6):805–20.
41. Boyapati RK, Dorward DA, Tamborska A, et al. Mitochondrial DNA is a pro-inflammatory damage-Associated Molecular Pattern Released during active IBD. Inflamm Bowel Dis. 2018;24(10):2113–22.
42. Zhu H, Kong B, Che J, et al. Bioinspired nanogels as cell-free DNA trapping and scavenging organelles for rheumatoid arthritis treatment. Proc Natl Acad Sci U S A. 2023;120(33):e2303385120.
43. Arezki Y, Harmouch E, Delalande F, et al. The interplay between lysosome, protein corona and biological effects of cationic carbon dots: role of surface charge titratability. Int J Pharm. 2023;645:123388.
44. Korkmaz A, Oyar EO, Yildirim Z, et al. Application of vascular endothelial growth factor at different phases of intestinal ischemia/reperfusion: what are its effects on oxidative stress, inflammation and telomerase activity? Adv Clin Exp Med. 2020;29(12):1417–24.
45. Zhang LL, Ding K, Liao SS, et al. Sestrin2 reduces ferroptosis via the Keap1/Nrf2 signaling pathway after intestinal ischemia-reperfusion. Free Radic Biol Med. 2024;214:115–28.
46. Karasawa S, Nakada TA, Sato M, et al. Early Elevation of cell-free DNA after Acute Mesenteric Ischemia in rats. J Surg Res. 2022;269:28–35.
47. Maryam B, Smith ME, Miller SJ, et al. Macrophage ontogeny, phenotype, and function in Ischemia Reperfusion-Induced Injury and Repair. Kidney360. 2024;5(3):459–70.
48. Boettcher M, Eschenburg G, Mietzsch S, et al. Therapeutic targeting of extracellular DNA improves the outcome of intestinal ischemic reperfusion injury in neonatal rats. Sci Rep. 2017;7(1):15377.
49. Zhang YN, Poon W, Tavares AJ, et al. Nanoparticle-liver interactions: Cellular uptake and hepatobiliary elimination. J Control Release. 2016;240:332–48.
50. Cymbaluk-Płoska A, Sobolewski P, Chudecka-Głaz A, et al. Double-emulsion Copolyester Microcapsules for Sustained Intraperitoneal Release of Carboplatin. J Funct Biomater. 2019;10(4):55.

Publisher's note